POWER LOSSES IN MASSIVE, SOLID, SATURABLE IRON

by

Earl Napoleon Fray

Thesis submitted to the Graduate Faculty of the

Virginia Polytechnic Institute

in candidacy for the degree of

MASTER OF SCIENCE

in

Electrical Engineering

June, 1962

Blacksburg, Virginia

I. INTRODUCTION

The total losses, which occur when iron is subjected to an alternating magnetization, are commonly considered to consist of two components. One is due to eddy-currents induced in the iron, and the other is due to magnetic hysteresis. Experimentally these two components are separated by measuring the total power, for a given flux density, at two or more frequencies and plotting the power loss per cycle versus frequency. The eddy-current loss is zero for zero frequency, hence extrapolating the curve to zero frequency gives the static hysteresis loss. It is then assumed that the hysteresis per cycle loss is constant for all frequencies, hence the eddy-current component is found by subtracting the hysteresis loss from the total. However if this apparent eddy-current loss is compared to the value calculated from the classical formulae, it is invariably found to be greater by a substantial factor. In some cases the measured loss is two or more times the calculated value.

In spite of the enormous amount of work done in this field in the past fifty years, no theoretically sound formula has been developed which would give the iron losses within engineering accuracy over a wide range of material thickness, applied magnetizing force, and frequency. The difficulty in deriving such a formula arises from the extremely non-linear relation between the magnetic intensity and the flux density, which the hysteresis loop represents

for a ferromagnetic material. Therefore, an exact mathematical derivation of the iron losses is not possible.

An approximate solution may be obtained by assuming the permeability to be a constant; however, this yields good results only if the material is being worked on the linear portion of the magnetization curve. It should be realized that even for weak magnetization, a close examination of the magnetization curve will show that the assumption of linearity in actual practical cases is not justified. Since the eddy-current losses as given by the linear theory are dependent on the value of permeability assumed, the results given by the linear theory have little quantitative meaning except to give a physical conception of the phenomenon.

In many applications the iron is saturated during the major portion of a cycle, formulae have been developed which appear satisfactory in this case. However, for the general situation where the eddy-current loss and the hysteresis loss are comparable, the theory is still obscure.

The equation to be considered is developed from Maxwell's equation.

A circular cylindrical rod of infinite length and radius r is the geometry considered. The excitation is applied in the form of a current sheet about the surface, hence the applied field is in the positive axial direction. Employing cylindrical coordinates, it is seen that eddy-currents will be induced in the negative tangential direction and the magnetization surface will move radially

from the sample surface toward the center. Applying Maxwell's equations, we get

$$\bar{\nabla} \times \bar{h} = \bar{j} = \sigma \bar{e} \qquad 1$$

and

$$\bar{\nabla} \times \bar{e} = - \frac{\partial}{\partial t} \bar{b} \qquad 2$$

where σ is the conductivity. From a consideration of symmetry, equations 1 and 2 reduce to

$$-\frac{\partial H_z}{\partial r} = \sigma E_\theta \qquad 3$$

and

$$\frac{\partial B_z}{\partial t} = \frac{1}{r} \frac{\partial}{\partial r} (r E_\theta) \qquad 4$$

Eliminating E_θ from equations 3 and 4 yields

$$\frac{\partial}{\partial t} B_z = \frac{1}{r} \frac{\partial}{\partial r} \left(\frac{r}{\sigma} \frac{\partial H_z}{\partial r} \right) \qquad 5$$

or, dropping the subscripts and rearranging, we get

$$\sigma \frac{\partial B}{\partial t} = \frac{\partial^2 H}{\partial r^2} + \frac{1}{r} \frac{\partial H}{\partial r} \qquad 6$$

The relation between the flux density and the magnetic intensity is given by the appropriate hysteresis loop. Due to the extreme non-linearity of this relation, a general solution of equation 6 does not exist.

Approximate solutions found in existing literature, to

equation 6, or a similar equation resulting from a different shape material, are reviewed in detail.

Finally, an appoximate solution is proposed which includes the effects of hysteresis as well as saturation.

All quantities herein are expressed in the rationalized meter-kilogram-second system of units. Vector quantities are written with a bar above them. For the sake of clarity any quantity which varies sinusoidally with time is indicated with a dot above it.

II. INVESTIGATION OF THE EDDY-CURRENT ANOMALY

A thorough investigation of the eddy-current anomaly has been made by Brailsford.[1] By comparison of experimental data with values computed by existing formulae, a better understanding of the nature of the problem is gained.

A rigid mathematical solution of the eddy-currents and flux distribution inside a sample of iron is not possible due to the non-linear relation between flux density and the magnetic intensity. If, however, the permeability is assumed constant; i.e. the hysteresis loop is assumed to be a single straight line, a solution may be obtained. This solution is well known and has been applied to many geometries, but with only limited success. Even without considering the complication of hysteresis, the permeability varies with flux density over a very wide range. Hence the above solution is meaningful only in a few restricted cases.

The apparent eddy-current loss as determined by the method described in the introduction, assumes that the hysteresis loss per cycle is not frequency dependent. The apparent eddy-current loss determined in this manner is always found to be greater than the eddy-current loss calculated using the assumption of constant permeability. This discrepancy for the particular samples used, ranged from 50 to 90 per cent.

This difference could be explained if the assumption that the hysteresis loss is independent of frequency is discarded. If, in fact, the hysteresis loss increases with frequency so that this

increase corresponds exactly to the anomalous loss, the difficulty would vanish.

Measurements have been made by Newmann[2] on two samples of unalloyed iron and on a sample of 4 per cent silicon steel, in which the calculated eddy-current loss was a very small portion of the total loss. This was accomplished by rolling the sheets very thin. The hysteresis loop for each of the samples was determined ballistically at 50 cycles per second. It was concluded, by comparison with the static hysteresis loops, that the loss at 50 cycles per second was 22 per cent greater for one sample and 46 per cent greater for other samples of iron. For the 4 per cent silicon steel, however, there was no measurable difference. These results indicate that it is not always possible to assume that the size of the hysteresis loop is independent of frequency. Even though the hysteresis loop for the silicon steel apparently did not vary with frequency, the anomaly being considered here is present to a high degree. Hence there must be other factors responsible for this discrepancy in addition to a possible change in the hysteresis loop. Two factors which may have a bearing on the anomaly, both causing distortion of the flux density and eddy-current waveform, will be considered.

It is well known that if strips are cut from a sheet of steel and the magnetization curves are measured, wide variations in the shape of the curves are found. This is true even when great care is taken to cut the sheets in the same direction as the rolling.

This non-uniformity of the magnetic material leads to a waveform distortion within the material which is different at each layer even though the total flux waveform is sinusoidal.

The second source of waveform distortion will occur even if the magnetic material is everywhere uniform in its magnetic properties. If in the calculations it is assumed that the permeability is a constant, and if a sinusoidal field is applied, the flux density and eddy-current at any point within the material is a pure sine wave. Clearly, if the waveform at any point in the material is sinusoidal, then, because of the extremely non-linear relation represented by the hysteresis loop, the applied field must be of distorted waveform. Thus, although the total flux within the material is sinusoidal, the waveform for any particle will be distorted, hence the hysteresis loop traversed will be different than that indicated by the total flux measurement. Clearly this distortion will affect the actual hysteresis and eddy-current loss. Furthermore, if the magnetization characteristics of the material varies from the surface to the center, then the distortion will be still worse.

The first source of waveform distortion is considered experimentally by taking sixteen strips of 4 per cent silicon steel, all cut from a single sheet. The measured magnetization curves are found to vary over a wide range. In the test, eight strips are placed in one leg of a Churcher[3] iron-loss tester. Each strip is closely wound with a search coil at its center, also an additional

search coil is wound on the entire packet. Similarly, the remaining eight strips are placed in the other leg. A sinusoidal frequency is then applied to the magnetizing windings of the tester for various values of flux density. The electromotive force induced in each search coil is observed on a cathode-ray oscillograph. The waveforms for each lamination are distorted to a high degree, whereas the applied waveform is sinusoidal, indicating that the total flux is sinusoidal. For a second test the strips are reshuffled and the above procedure is repeated.

There will be a change in the iron loss in any strip having a distorted waveform, when compared with that for a sine wave, due to two causes. First, the distortion causes a change of the eddy-current waveforms and hence the eddy-current loss. Second, the hysteresis loss depends on the amplitude of the flux wave which, in general, differs from the value for the sine wave which would exist if there is no distortion. However, a careful analysis of the waveforms reveal that, in spite of the severe distortion, the effect on the total iron loss is to increase it by only about one per cent above the value which would be obtained if the flux in each lamination had been sinusoidal. Therefore, the non-uniformity of magnetic characteristics cannot be responsible for the anomalous eddy-current loss in spite of the severe waveform distortion.

To consider internal waveform distortion due to eddy-currents and to the non-linear relation between the flux density and the magnetic intensity, an experimental model designed to represent a single sheet of iron is developed. Figure 1 represents a section

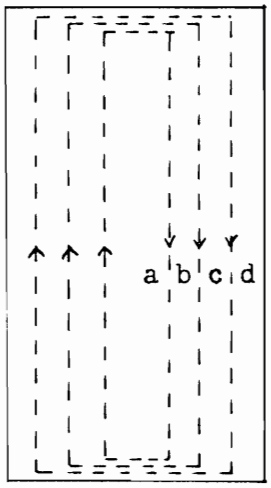

Figure 1 Single sheet

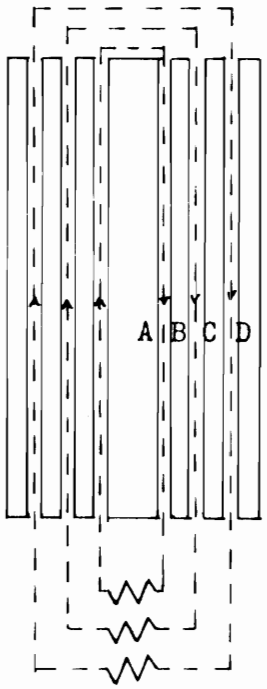

Figure 2 Experimental model

through an iron sheet and Figure 2 represents the corresponding experimental model. If an alternating flux is applied in a direction normal to the section, eddy-current paths will be parallel to the surface of the sheet. A few of the paths are shown by dashed lines.

At the surface of the material, the only forces acting are those produced by the external field; however, at a point within, the value of the field acting is the instantaneous sum of the applied field and the field set up by the eddy-currents which encircle the point. Although the total flux in the sheet may be sinusoidal, it is not possible, in general, for the flux at any point within the sheet to be sinusoidal. If, the relation between the flux density and the magnetizing force being given by the appropriate hysteresis loop, the flux is everywhere a sine wave, then the externally applied field must have a distorted waveform. Since the eddy-currents will be sinusoidal, the field at the center of the sheet will be the sum of the sinusoidal eddy-current field and the distorted external field. Therefore the waveforms of the fields acting at the surface and at the center will be different. In fact, if the externally applied field is sinusoidal, there must be a gradual transition from surface to center in such a manner that the total flux is sinusoidal.

The amount of distortion within the sheet will depend on the strength of the eddy-current field relative to the applied field. Hence the distortion will be a function of the thickness, permeability, and conductivity of the sheet as well as frequency.

The distortion of the internal flux leads to a distortion

of the eddy-current waveform which in turn may cause a discrepancy between the calculated and actual eddy-current loss. What may be even more important is the fact that the flux distortion may lead to a significant change in the hysteresis loss per cycle with frequency. If the frequency is increased the eddy-currents will increase, resulting in an increased distortion of the internal flux waveform. Since the hysteresis loss in any particle will depend on the maximum flux density occuring in it, the increased distortion will alter the amplitude of the flux waveform and the resulting hysteresis loss per cycle. Hence in the separation of the losses by the method already mentioned, the apparent eddy-current loss may not be the eddy-current loss alone, but may contain a frequency dependent increase of hysteresis loss due to flux distortion.

Figure 1 represents a section through a single sheet. It is desired to determine the flux density and eddy-current waveforms at any point within the sheet for alternating magnetization. Since this can not be done a model is made as shown in Figure 2.

The model consists of sixteen sheets of silicon steel subdivided into four packets of four strips each. The inner packet is wound with 200 turns of insulated copper wire. The second packet is placed on one side of the inner packet and a further 200 turns is wound to embrace both packs. The third and fourth packets are added in the same manner. The windings are represented by the dashed lines and are used to allow circulating currents of variable magnitude to flow, corresponding to eddy-currents in an actual

sheet. In addition, each pack is wound with a search coil for the determination of the electromotive force and flux waveform.

For the model to be an accurate representation of a single sheet, the following appear to be the main requirements:

1. The material of the model should have a hysteresis loss and magnetization characteristics approximating the sheet being simulated. The eddy-current loss should be negligible.

2. The artificial eddy-currents should be produced by a large number of windings, each connected to an external resistive load.

3. Great effort should be made to make all other disturbing influences as small as possible.

Comparison of Figure 1 and Figure 2 shows that the center of the material is acted on by the external field and the field due to the actual eddy-current or the artificial eddy-currents respectively.

Thus, it is possible to investigate the effects of eddy-currents within the sheet by examining the conditions in the corresponding part of the model. It is apparent the approximation becomes better as the number of sections becomes greater.

Measurements made of the total iron loss in the model with the eddy-current windings open-circuited reveal that the hysteresis loss component is 94.5 per cent of the total. Therefore condition one is approximately fulfilled.

Thus it may be supposed that the flux waveforms as determined in the packs A, B, C, D in Figure 1 will approximately

correspond to the flux waveform occuring in the sheet at the points a, b, c, d in Figure 2. Obviously, since the flux distribution in the model proceeds in discontinuous steps, the results obtained are a first approximation only.

The model is placed in one leg of an iron-loss tester, and the waveforms are determined on a cathode-ray oscillograph after one stage of amplification. Since only a resistive load is used, the eddy-current waveforms are the same as the corresponding electromotive force waveforms.

The eddy-current waveforms at five points from the center to the surface of the model are given in Figure 3. The upper curves are calculated using an assumption of constant permeability. The lower curves are waveforms observed from the model. An analysis of the eddy-current flowing one quarter of the distance from the center to the surface (curve b) reveals the following harmonic content, expressed as a percentage of the fundamental.

3rd harmonic = 55%

5th harmonic = 21%

7th harmonic = 7%

The distortion of the eddy-current waveforms leads to a modification of the actual eddy-current loss. The effect of this distortion is estimated to be small and, in fact, negligible.

However, the effect of the distortion on hysteresis loss is found to be significant. The measured values of the amplitude of the flux density differ greatly from the mean flux density, which in turn causes an increase of the hysteresis loss per cycle as the

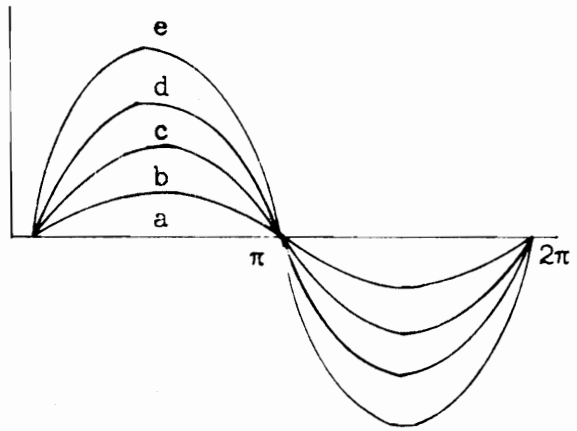

(A)

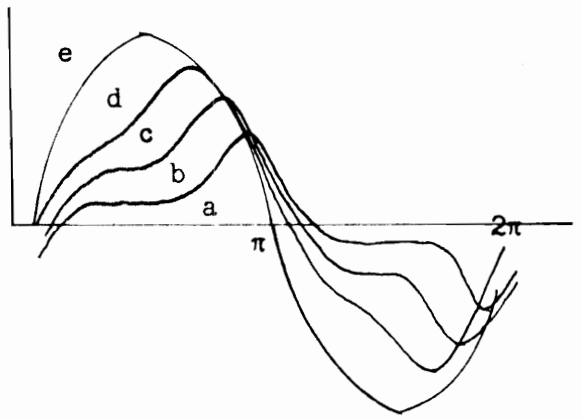

(B)

Figure 3 Density of eddy-currents at different points in the section of sheet steel

(A) Values calculated using assumption of constant permeability
(B) Observedcurves on experimental model

frequency is increased. It is found for one sample tested that the hysteresis loss per cycle at 50 cps was 13.9 per cent greater than the static value. This agreed very closely with the measured loss.

It is clear that, contrary to the usual assumption, the hysteresis loss per cycle will be frequency dependent due to internal waveform distortion.

III. DETERMINATION OF LOSSES IN MASSIVE IRON BY LIMITING NON-LINEAR THEORY

An analysis[4] is given below for the solution to the basic Maxwell equations when the magnetizing force is very large, so that complete saturation takes place. A formula for the input power is developed and compared with the formula by Rosenberg[5].

The assumed magnetization curve is shown in Figure 4, which shows that the flux density will be a constant for any magnetizing force.

Using this curve and a semi-infinite sea of metal, consider the electric field as having only an x-component, and the magnetic field and magnetizing force as acting only in the y-direction.

The magnetic intensity at the surface is given as

$$H = H_0 \sin \omega t \qquad 7$$

also, at the surface (z = 0) the electric field intensity e and the flux density b are designated as E, B. For the above conditions, Maxwell's equations become

$$-\frac{\partial \bar{h}}{\partial z} = \sigma \bar{e} \qquad 8$$

$$\frac{\partial \bar{e}}{\partial z} = -\frac{\partial \bar{b}}{\partial t} \qquad 9$$

At an infinite depth ($z = \infty$), all fields are defined as zero. With this, the boundary conditions are defined. Due to the possibility that the time rate of change of the electric field may be infinite, equation

9 is replaced by its integral with respect to z; hence the following is defined:

$$\bar{\phi} = \int_{z}^{\infty} \bar{b} \cdot d\bar{z} \qquad 10$$

Thus, Maxwell's equations become

$$-\frac{\partial \bar{h}}{\partial z} = \sigma \bar{e} \qquad 11$$

$$\bar{e} = \frac{\partial \bar{\phi}}{\partial t} \qquad 12$$

In preference to a direct analytical solution, a field configuration will be chosen and proved that it satisfies equations 11 and 12 with the given boundary conditions. This field configuration is shown in Figure 5. For a depth of penetration greater than δ, all fields are assumed zero. The value of the flux density is taken as

$$B = B_o \ Sig \ H \qquad 13$$

where "Sig H" means "Sign of H", and is the unit square wave associated with the magnetic intensity. The point where the magnetic intensity and flux density changes sign is designated as

Thus, the assumed field configuration has been forced to satisfy the boundary conditions, and only equations 11 and 12 remain to be satisfied. From Figure 5, it is noted that

$$-\frac{\partial h}{\partial z} = \frac{H}{\delta} \qquad 14$$

therefore, equation 11 becomes

$$\frac{H}{J} = \sigma E \qquad 15$$

also for $z < \ell$ it is noted

$$\frac{\partial \phi}{\partial t} = 2B \frac{d\ell}{dt} = e = E \qquad 16$$

and for $z > \ell$

$$\frac{\partial \phi}{\partial t} = 0 \qquad 17$$

thus, equation 12 is completely given by equation 16; i.e.:

$$E = 2B \frac{d\ell}{dt}$$

Equations 15 and 16 are dependent only on time and $E_{(t)}$ and $\ell_{(t)}$ are the unknowns. Eliminating E yields,

$$2\ell \frac{d\ell}{dt} = \frac{H}{\sigma B} \qquad 18$$

or letting

$$H = H_o \sin \omega t$$

we get

$$\frac{d}{dt}(\ell)^2 = \frac{H_o}{\sigma B_o} |\sin \omega t| \qquad 19$$

Remembering that the magnetic intensity and the flux density must always be of the same sign, equation 19 indicates that ℓ must always be positive. This seems unusual and is justified by the

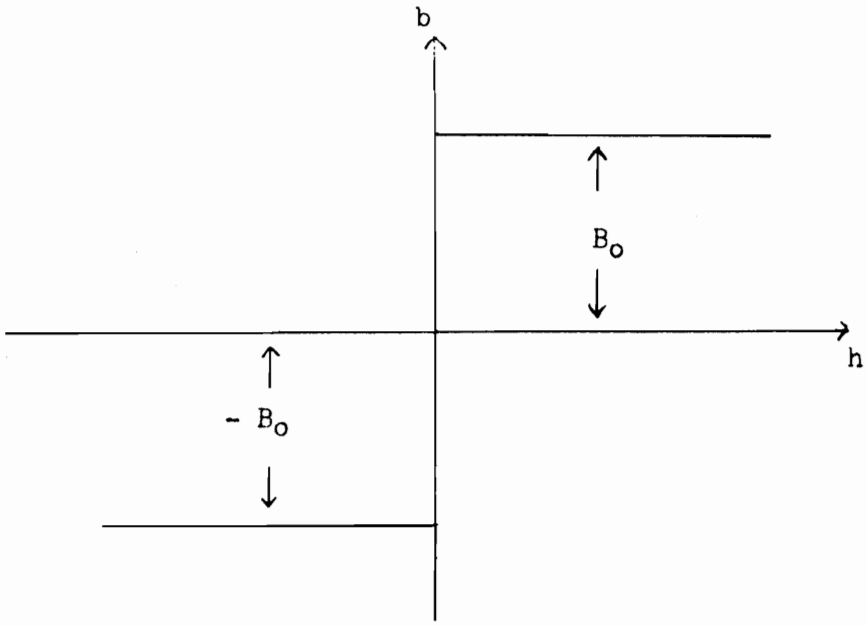

Figure 4 Assumed B-H curve

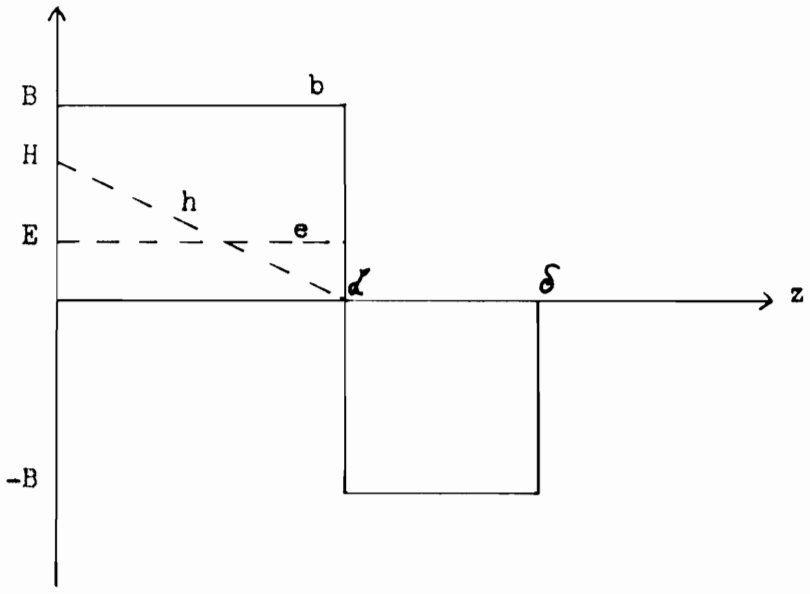

Figure 5 Proposed field configuration

following argument. To see this is so, consider any node of H. If $\mathcal{I}$ were not zero just after this instant, the sign reversal of H would cause a finite jump in the flux density over a finite region and hence cause a finite jump in the flux at the surface, resulting in the electric field being infinite which is clearly impossible. Consequently, $\mathcal{I}$ must be zero just following each node of H. From this it is concluded that each half cycle is the same.

For the first half cycle $\mathcal{I}_{(x)}$ is calculated from equation 19.

$$\frac{d}{dt}(\mathcal{I})^2 = \frac{H_o}{\sigma B_o} \sin \omega t \tag{20}$$

$$\mathcal{I}^2 = \frac{H_o}{\sigma B_o}\left(-\frac{\cos \omega t}{\omega}\right) + K$$

at

$$t = 0$$

$$\mathcal{I} = 0$$

hence

$$K = \frac{H_o}{\sigma B_o \omega} \tag{21}$$

thus

$$\mathcal{I}^2 = \frac{H_o}{\sigma B_o}\left(\frac{1 - \cos \omega t}{\omega}\right)$$

$$\mathcal{I} = \left(\frac{2 H_o}{\sigma B_o \omega}\right)^{1/2} \sin \frac{\omega t}{2} \qquad , \quad 0 < \omega t < \pi \tag{22}$$

From this δ can be computed which is the extreme value of $\mathcal{I}$ or the "depth of penetration" for each half period.

$$\delta = \left(\frac{2}{\omega \sigma (B_o/H_o)} \right)^{1/2} \qquad 23$$

By combining equations 15, 22 and 23, the equation for E becomes

$$E = \frac{H_o \sin \omega t}{\sigma \delta \sin \frac{\omega t}{2}} \quad , \quad 0 < \omega t < \pi$$

which reduces to

$$E = \frac{H_o}{\sigma \delta} \cos \frac{\omega t}{2} \quad , \quad 0 < \omega t < \pi \qquad 24$$

Investigation of equation 15 reveals that if in successive half periods, H reverses and δ does not, then E must reverse. A plot of $\delta(t)$ and $E(t)$ is shown in Figure 6. The determination of E completes the proof that Figure 4 is the solution for the boundary conditions stated.

To compute the power per unit area in the metal, consider the Poynting Vector

$$\bar{N} = N + jM = \frac{1}{2} \bar{E} \bar{H}^* \qquad 25$$

where E and H are the peak complex amplitudes of H and E. The asterisk means complex conjugate. Hence the real part of equation 25 would be the power flow. The wave impedance $\bar{\eta}$ at the surface is defined as

$$\bar{\eta} = r + jx = \frac{\bar{E}}{\bar{H}} \qquad 26$$

hence

$$N = \frac{1}{2} r H_o^2 \qquad 27$$

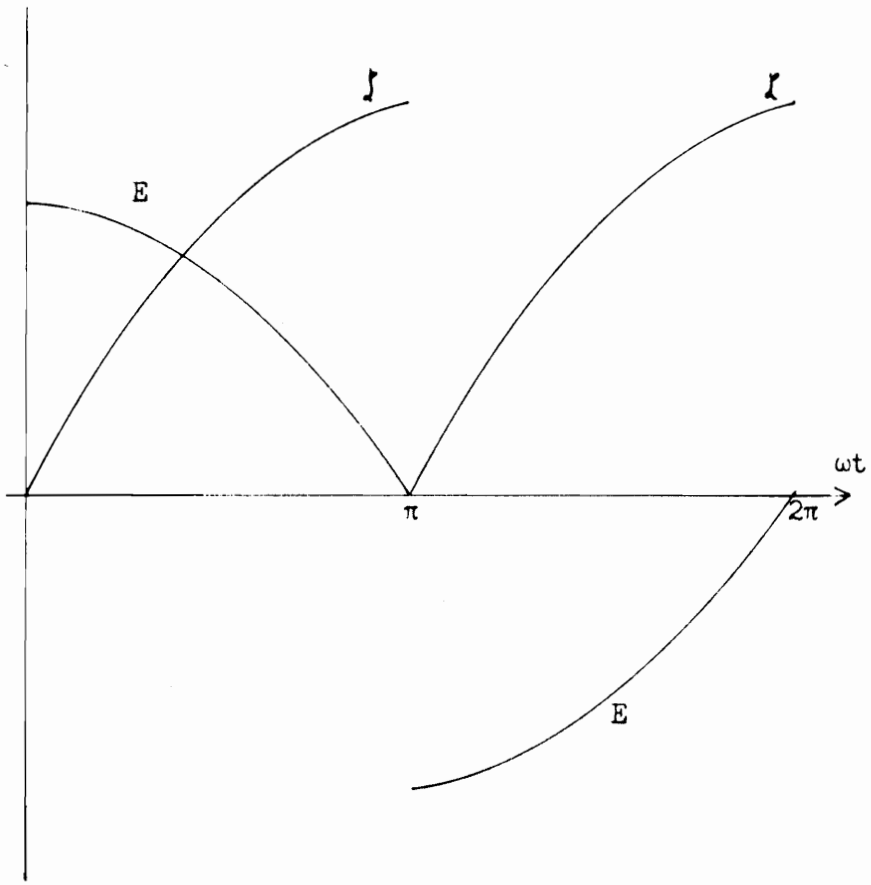

Figure 6 Plot of waveshapes of E and

therefore the power flow can be readily determined by the determination of r.

To do this, we must remember that only the fundamental of E contributes to the power flow. Hence by Fourier series E is found, and equation 26 is solved for r.

$$E = 2 \sum_{1}^{\infty} (A_N \cos N\omega t + B_N \sin N\omega t)$$

where

$$A_N = \frac{1}{T} \int_0^T E(t) \cos N\omega t \, dt$$

$$B_N = \frac{1}{T} \int_0^T E(t) \sin N\omega t \, dt$$

hence for $N = 1$

$$A_1 = \frac{2 H_0}{\sigma \delta \pi} \int_0^{\pi} \cos \frac{\omega t}{2} \cos \omega t \, d(\omega t) \qquad 28$$

$$B_1 = \frac{2 H_0}{\sigma \delta \pi} \int_0^{\pi} \cos \frac{\omega t}{2} \sin \omega t \, d(\omega t) \qquad 29$$

By using the following identities

$$\cos\alpha \cos\beta = \frac{1}{2} \cos(\alpha - \beta) + \frac{1}{2} \cos(\alpha + \beta)$$

$$\sin\alpha \cos\beta = \frac{1}{2} \sin(\alpha + \beta) + \frac{1}{2} \sin(\alpha - \beta)$$

equations 28 and 29 reduce to

$$A_1 = \frac{H_0}{\sigma \delta \pi} \int_0^{\pi} (\cos \tfrac{3}{2}\omega t + \cos \tfrac{1}{2}\omega t) d(\omega t) = \frac{4 H_0}{3 \sigma \delta \pi} \qquad 30$$

$$B_1 = \frac{H_0}{\sigma \delta \pi} \int_0^{\pi} (\sin \tfrac{3}{2}\omega t + \sin \tfrac{1}{2}\omega t) d(\omega t) = \frac{8 H_0}{3 \sigma \delta \pi} \qquad 31$$

and therefore

$$E = \frac{8}{3}\frac{H_0}{\sigma\delta\pi}\left(\cos\omega t + 2\sin\omega t\right)+\cdots \qquad 32$$

so

$$\bar{E} = \frac{8H_0}{3\sigma\delta\pi}(1-j2) \qquad 33$$

and

$$\bar{H} = -jH_0 \qquad 34$$

whence

$$\bar{\eta} = \frac{\bar{E}}{\bar{H}} = \frac{8}{3\sigma\delta\pi}(2+j1) \qquad 35$$

and

$$r = \frac{16}{3\sigma\delta\pi} \qquad 36$$

when equation 23 is substituted for δ, equation 36 becomes

$$r = \frac{16}{3\pi}\left(\frac{\omega B_0/H_0}{2\sigma}\right)^{1/2} \qquad 37$$

Thus, at complete saturation, the power input would be

$$N = \frac{8}{3\pi}\left(\frac{\omega B_0/H_0}{2\sigma}\right)^{1/2}H_0^2 \qquad 38$$

Mac Lean's equation 36, when compared with the work of Rosenberg[5], is found to differ only by $\pi/4$; i.e.:

$$r_{\text{Rosenberg}} = \frac{\pi}{4}\, r_{\text{Mac Lean}}$$

Comparison of equation 37 with the equivalent formula for non-ferrous materials reveals that the only difference is the factor $16/3\pi$, this factor is termed the "ferrous multiplier". However it is apparent that if there is not complete saturation, the "ferrous multiplier" would lie between unity and $16/3\pi$. It would appear then that Rosenberg's "ferrous multiplier" is $4/3$, which lies about midway between the linear and rectangular case.

IV. LIMITING NON-LINEAR THEORY EXTENDED TO INCLUDE THIN PLATES

Many authors[4,6,7] have used the rectangular B-H curve assumption for computing the losses in iron. In particular, Mac Lean[4] has used a very similar analysis to derive a formula for the solid iron case. The analysis[8] considered here is in effect an extension of Mac Lean's work in that thin plates are considered, thus yielding a general formula.

The assured magnetization curve for which the analysis is made is shown in Figure 4.

An iron plate of infinite X and Y dimensions and a thickness of 2d in the z-direction is to be considered.

A sinusoidal magnetizing force $H = H_0 \sin \omega t$ in the y-direction is maintained on each face of the plate. There is no variation of H in the x-direction, hence the resulting electric field will be normal to magnetic field and in the x-direction. Consequently, x-polarized plane waves propagate from the surfaces toward the center of the plate. Since the plate is symmetrical, only one half of the plate thickness need be considered. As the waves penetrate the plate they are alternated; however, due to the assumed B-H curve, the changes in magnetization take place only at the front of the wave[4]. The wave front with h increasing is accompanied by a flux density wave of constant amplitude B_0. The extreme depth to which the fields penetrate is called the "depth of penetration". This point is designated δ.

It is apparent two cases must be considered. One where $\delta > d$; in this case the two flux waves would penetrate until they met in center, for the remaining half period the flux will remain constant. In case two, where $\delta < d$, the waves penetrate to the depth δ and the inner portion of the plate remains unmagnetized.

For the negative half cycle the above described wave penetration would repeat, only now the flux-density wave would be of constant amplitude $-B_o$. Thus the direction of magnetization is reversed in each half period. This point of reversal is designated $\mathcal{L}(t)$ and is termed as the "separating surface".

Figure 8 illustrates the above described field configuration.

Maxwell's equations in integral form, neglecting displacement current, are

$$\oint \bar{h} \cdot d\bar{l} = \sigma \int_s \bar{e} \cdot d\bar{s} \qquad 39$$

$$\oint \bar{e} \cdot d\bar{l} = \frac{\partial}{\partial t} \int_s \bar{b} \cdot d\bar{s} \qquad 40$$

where σ is the conductivity and all variables are expressed in RMKS units.

For the problem stated, the electric field has only an x-component and magnetic intensity and flux density have only y-components, thus equations 39 and 40 become

$$\oint \bar{h}_y \cdot d\bar{l} = \sigma \int_s \bar{e}_x \cdot d\bar{s} \qquad 41$$

$$\oint \bar{e}_x \cdot d\bar{l} = -\frac{\partial}{\partial t}\int_s \bar{b}\cdot d\bar{s} = -\frac{\partial}{\partial t}\Phi \qquad 42$$

where ϕ is the flux through the surface for the line integral taken.

The values of the variables at the surface are defined as E, B, and H. For $H = H_0$ Sin ωt the flux density may be written as

$$B = B_0 \text{ Sig } H$$

where "Sig H" means "Sign of H".

Referring to Figure 8, at any instant the separating surface at depth f is moving with velocity v, hence in a time dt the flux

$$\phi = B_0 v\, dt$$

is built up while the flux from the previous half cycle is destroyed. Therefore

$$\frac{d\phi}{dt} = 2 B_0 v \qquad 43$$

for unit length in the x-direction.

To evaluate the line integral in equation 42 consider the closed loop abmc in Figure 9. The flux is not changing beyond the separating surface, consequently there is no electric field in this area.

The area enclosed by cmgf contains the separating surface, thus from equations 42 and 43

$$e_{cm} + e_{gs} = 2 B_0 v \qquad 44$$
$$= 2 B_0 \frac{df}{dt}$$

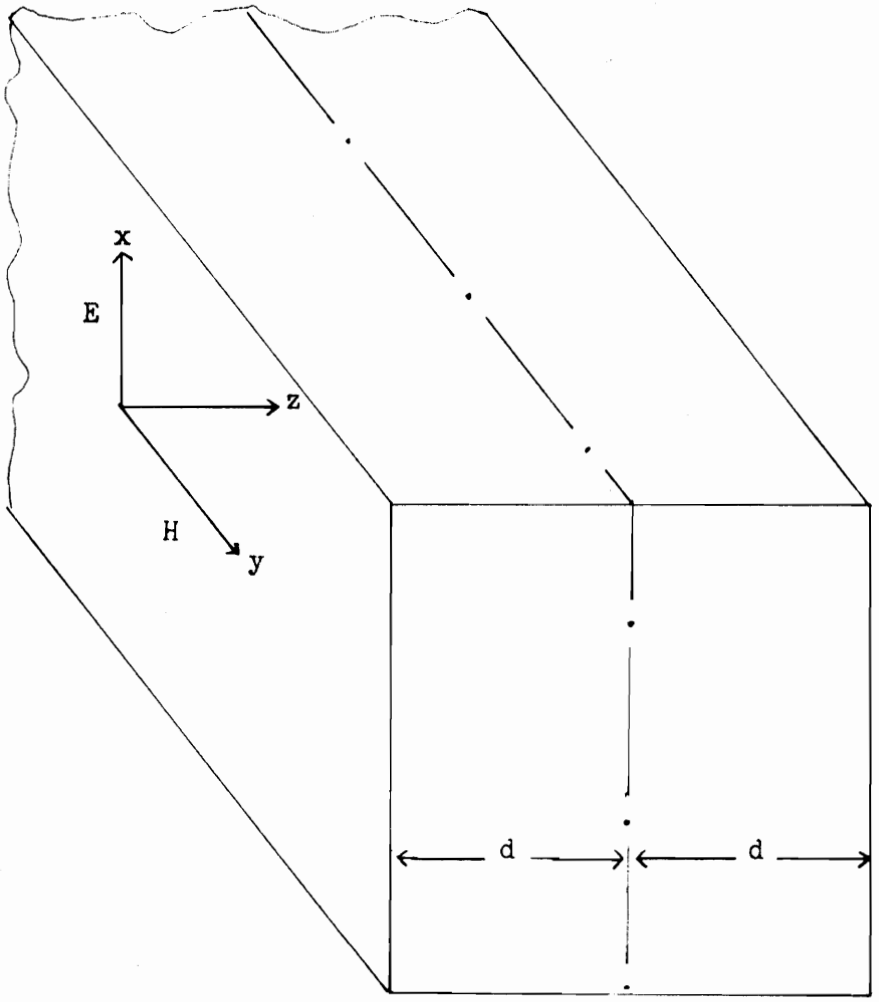

Figure 7 Plane waves penetrating inward from both faces of plate of thickness 2d

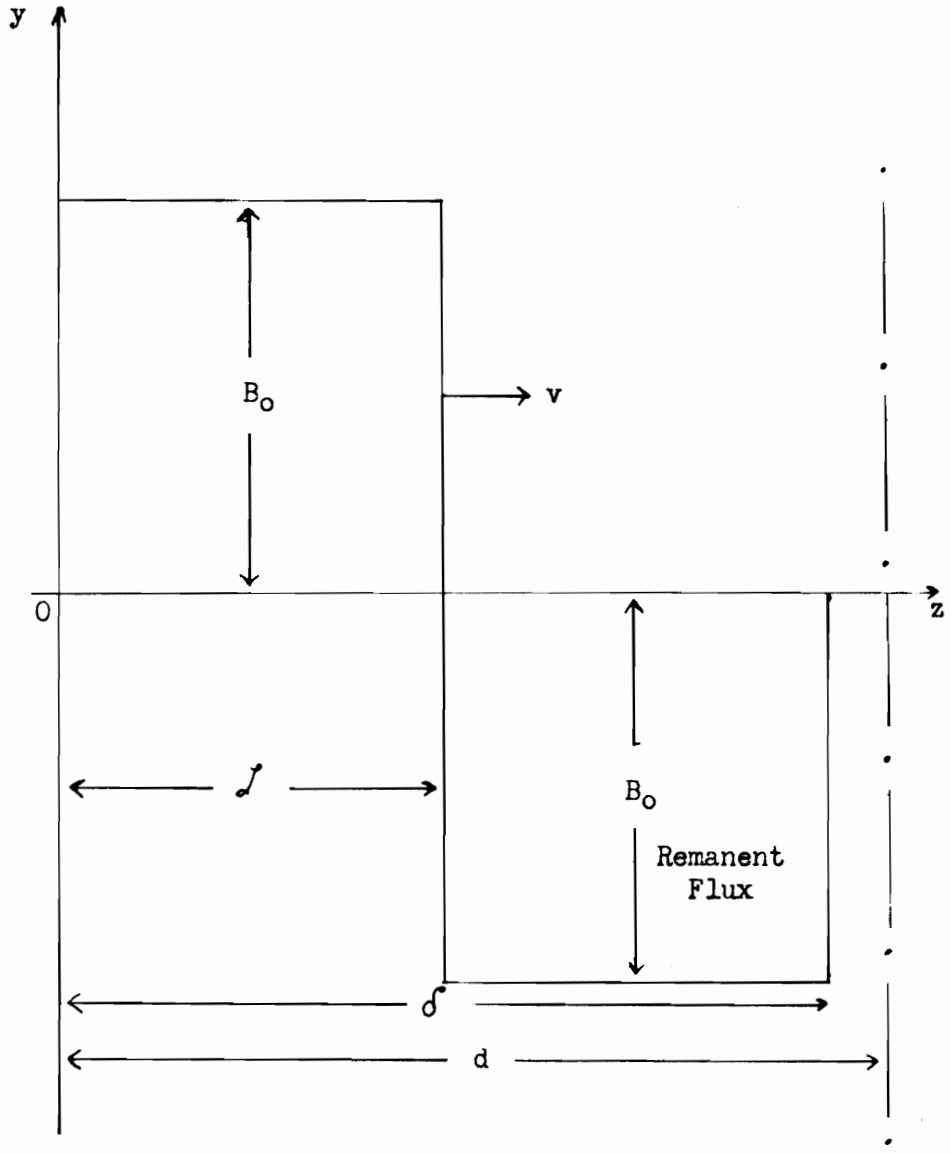

Figure 8 Separating surface penetrating the plate

or since $e_{cm} = 0$

$$e_{gf} = 2B \cdot \frac{dz}{dt} \qquad 45$$

The flux to the left of f is not changing, hence from loop fghk it is seen that

$$e_{fg} + e_{kh} = 0 \qquad 46$$

$$e_{hf} = e_{fg} = E$$

This shows for $0 < z < z_1$ the electric field is constant, and abruptly becomes zero at the separating surface.

For the evaluation of the line integral in equation 42, consider the loop abcf in Figure 10. At the separating surface, h is zero and at the surface of the material h equals H. There is no component of h in the z-direction, therefore

$$\oint_{abcf} \bar{h} \cdot d\bar{l} = H \qquad 47$$

giving

$$\frac{\partial h}{\partial z} = \frac{H}{f} = \sigma E \qquad 48$$

From equations 46 and 48, the following is concluded:

1. A uniform density of eddy-currents exist in the region $0 < z < f$ and are zero beyond.

2. The magnetic intensity decreases linearly from H at the surface of the material to zero at the separating surface, and is zero beyond.

3. The electric field intensity in a constant amplitude E

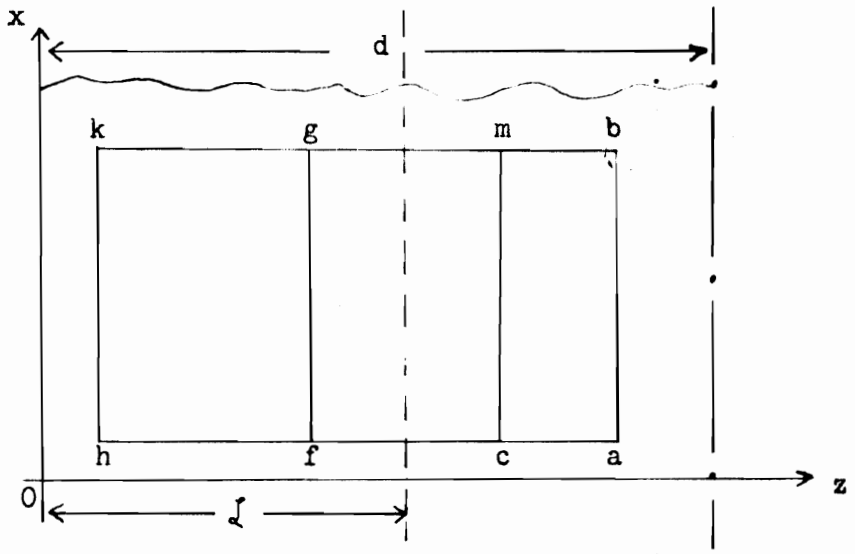

Figure 9 XZ section of the plate

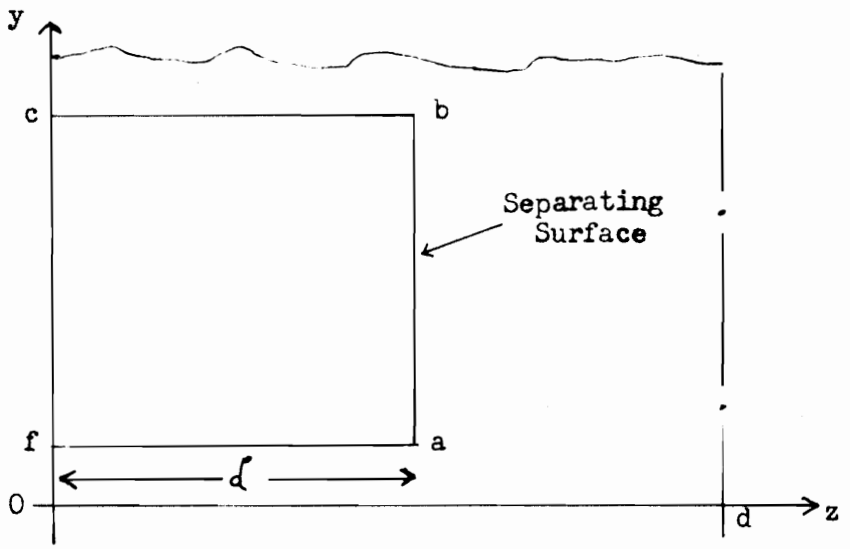

Figure 10 YZ section of the plate

for the region $0 < z < \delta$ and is zero beyond.

Figure 11 illustrates the field configuration at four instants of time, as indicated in Figure 11A. From consideration of Figure 11B, equation 48 becomes

$$\frac{\partial h}{\partial z} = \frac{H}{\delta} = \sigma E \quad , \delta < d \quad , \quad 0 < t < t_c$$
$$= 0 \quad , \quad t_c < t < \pi/\omega \qquad 49$$

This means, as shown in Figure 11C, that after time t_c, h becomes uniform throughout the plate at the value H. After half a cycle the magnetic intensity at the surface is zero, and is zero everywhere in the material. Thereafter a new separating surface starts from the two sides, as shown in Figure 11E.

Therefore Maxwell's equations are

$$\frac{H}{\delta} = \sigma E \quad , \quad 0 < t < t_c \qquad 50$$

$$E = 2 B_0 \frac{d\delta}{dt} \qquad 51$$

or

$$h = H \quad , \quad t_c < t < \pi/\omega$$
$$h = 0$$

Combining equations 50 and 51 and eliminating E, we get

$$2\delta \frac{d\delta}{dt} = \frac{H}{\sigma B} = \frac{H_0 \sin \omega t}{\sigma B_0 \, sig \, H}$$

or

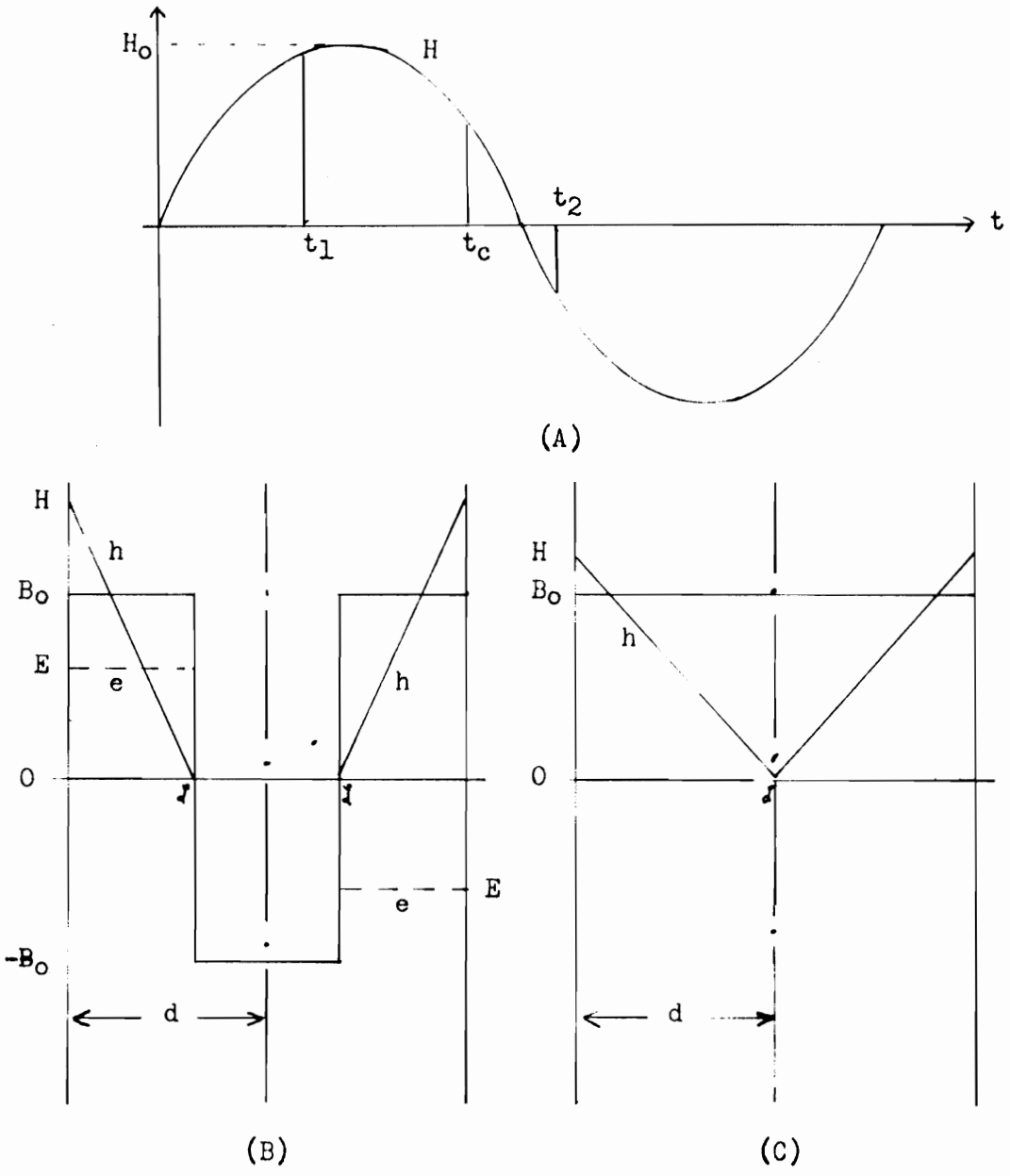

Figure 11 Description on Page 37

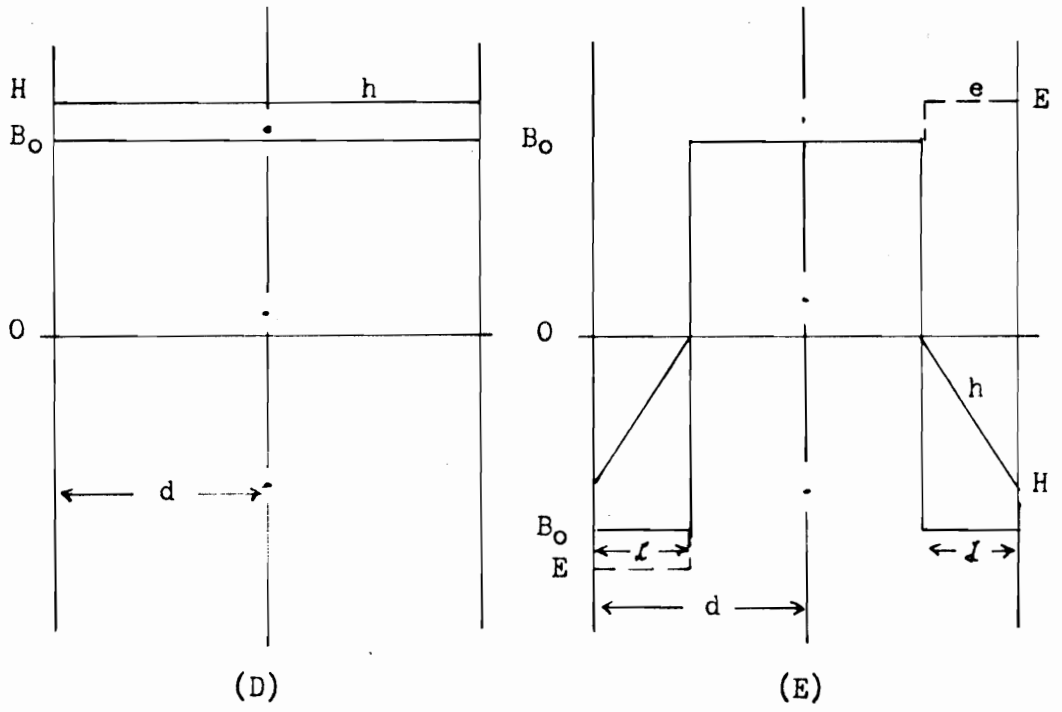

Figure 11 **Field configurations at four different instants**

(A) Mmf wave
(B) Flux has penetrated to depth ℓ. $\ell < d$, $t = t_1$
(C) Flux waves have just reached the center of the plate. $\ell = d$, $e = 0$, $t = t_c(-)$
(D) After the flux wave has reached the center of the plate, h becomes uniform. $h = H$, $e = 0$, $t = t_c(+)$
(E) New magnetic flux wave has penetrated for a distance ℓ, $t = t_2$
t_c = the instant at which separating surfaces reach the middle of the plate

$$\frac{d}{dt}(\delta)^2 = \frac{H_0}{\sigma B_0}\,|\sin \omega t| \qquad 52$$

From this equation it is seen that the separating surface must always move from the surface toward the center of the plate where it ceases to exist, and repeats every half-cycle when H becomes zero at the surface.

Consider the case where the plate thickness is greater than the depth of penetration δ. The motion of the separating surface, in the first half period, can be found as follows:

$$\frac{d(\delta)^2}{dt} = \frac{H_0}{\sigma B_0}\sin \omega t \qquad , \omega t < \pi$$

$$\delta^2 = \int_0^t \frac{H_0}{\sigma B_0}\sin \omega t\, dt \qquad 53$$

giving

$$\delta^2 = \frac{2H_0}{\omega \sigma B_0}\sin^2 \frac{\omega t}{2} \qquad , 0 < t < \pi/\omega \qquad 54a$$

where the depth of penetration is the maximum value of δ which is obtained at the end of each half period. Therefore

$$\delta = \left(\frac{2H_0}{\omega \sigma B_0}\right)^{1/2} = \left(\frac{2}{\omega \sigma B_0/H_0}\right)^{1/2} \qquad 54b$$

The solution of the problem for a thin plate follows exactly the solution for the thick plate, since the wave cannot tell whether it is penetrating a thick plate or thin plate until it meets the wave from the other side.

Therefore

$$\delta = \left(\frac{2 H_0}{\sigma \omega B_0}\right)^{1/2} \sin \frac{\omega t}{2} \quad , 0 < t < t_c$$

$$= \delta \sin \frac{\omega t}{2} \qquad (55)$$

hence

$$d = \delta \sin \frac{\omega t_c}{2} \qquad (56)$$

where t_c is the time when the separating surface reaches the middle, thus

$$t_c = \frac{2}{\omega} \sin^{-1} \frac{d}{\delta} \qquad (57)$$

From equation 50, E can be calculated.

$$E = \frac{H_0 \sin \omega t}{\sigma \delta \sin \frac{\omega t}{2}} \quad , 0 < t < t_c$$

$$= 0 \quad , t_c < t < \pi/\omega \qquad (58)$$

This may also be written

$$E = \frac{2 H_0}{\sigma \delta} \cos \frac{\omega t}{2} \quad , 0 < t < t_c$$

$$= 0 \quad , t_c < t < \pi/\omega \qquad (59)$$

A plot for H, E, and δ for thin plots and solid iron are given in Figure 12A and 12B respectively.

The power loss per unit area can be determined from the Poynting vector

$$\bar{N} = N + j M = \frac{1}{2} \bar{E} \bar{H}^* \qquad (60)$$

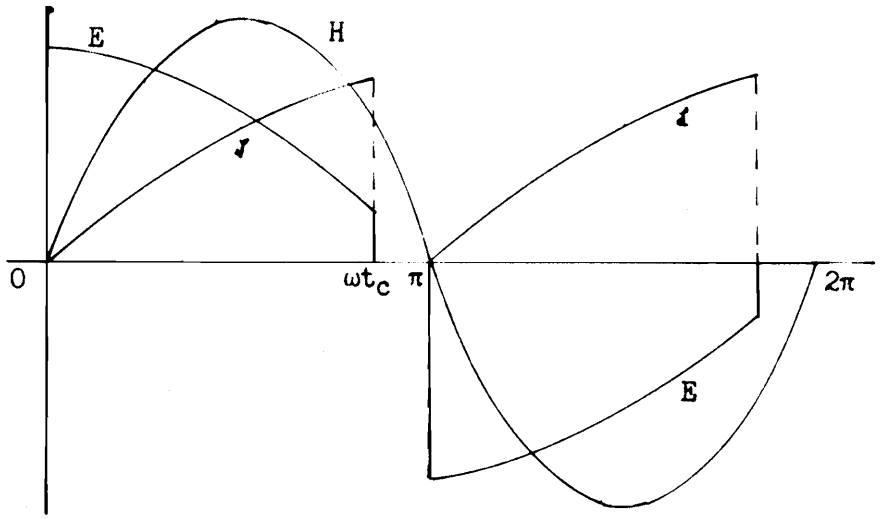

(A)

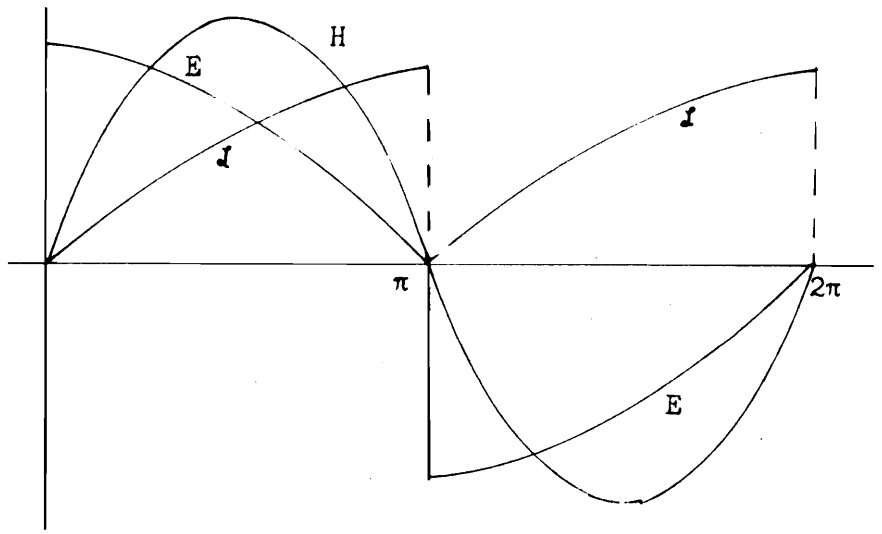

(B)

Figure 12 Plots of waveshape

(A) H, E, and J
(B) H, E, and J for the solid iron case

where E and H are the peak complex magnitudes of the fundamental component of E and H. Since H is sinusoidal, the harmonics of E do not contribute to the power flow. The real part of N gives the power flow.

The wave impedance at the surface can be written as

$$\bar{\eta} = r + j\chi = \frac{\bar{E}}{\bar{H}} \qquad 61$$

which yields

$$N = R_e\ \bar{N} = \frac{1}{2} r H_o^2 \qquad 62$$

In order to determine $\bar{\eta}$ it is necessary to find the value of E.

Considering equation 59 and Figure 9, the Fourier coefficients for the fundamental of E are found as follows:

$$A_1 = \frac{2H_o\omega}{\sigma\delta\pi}\int_0^{t_c}\left(\cos\frac{\omega t}{2}\cos\omega t\right)dt$$

$$= \frac{2H_o}{\sigma\delta\pi}\left(\frac{1}{3}\sin\frac{3}{2}\omega t_c + \sin\frac{1}{2}\omega t_c\right) \qquad 63$$

$$B_1 = \frac{2H_o\omega}{\sigma\delta\pi}\int_0^{t_c}\left(\cos\frac{\omega t_c}{2}\sin\omega t\right)dt$$

$$= \frac{2H_o}{\sigma\delta\pi}\left(\frac{4}{3} - \frac{1}{3}\cos\frac{3}{2}\omega t_c - \cos\frac{1}{2}\omega t_c\right) \qquad 64$$

Using equation 56 reduces these to

$$A_1 = \frac{4H_o d}{\delta\sigma\pi}\left[1 - \frac{2}{3}\left(\frac{d}{\delta}\right)^2\right] \qquad 65$$

and

$$B_1 = \frac{8 H_0}{3\sigma\delta\pi}\left[1 - \left(1 - \frac{d^2}{\delta^2}\right)^{3/2}\right] \qquad 66$$

Hence the fundamental of E is

$$E_1 = \frac{8H_0}{3\sigma\delta\pi}\left[3\frac{d}{\delta} - 2\frac{d^3}{\delta^3}\cos\omega t + 2\left\{1 - \left(1 - d^2/\delta^2\right)^{3/2}\right\}\sin\omega t\right] \qquad 67$$

and the peak complex amplitude of E and H is given by

$$\bar{E} = \frac{8H_0}{3\sigma\delta\pi}\left[3\frac{d}{\delta} - 2\frac{d^3}{\delta^3}\right) - j2\left(1 - \left(1 - \frac{d^2}{\delta^2}\right)^{3/2}\right)\right] \qquad 68$$

and

$$\bar{H} = -j H_0 \qquad 69$$

Therefore

$$\bar{z} = r + jx = \frac{\bar{E}}{\bar{H}}$$

$$= \frac{16}{3\sigma\delta\pi}\left[\left(1 - \left(1 - \frac{d^2}{\delta^2}\right)^{3/2}\right) + \frac{1}{2}j\left(3\frac{d}{\delta} - 2\frac{d^3}{\delta^3}\right)\right] \qquad 70$$

The phase angle of the impedance is

$$\tan\theta = \frac{3\frac{d}{\delta} - 2\frac{d^3}{\delta^3}}{2\left[1 - \left(1 - d^2/\delta^2\right)^{3/2}\right]} \qquad 71$$

Therefore, the power factor is given by

$$pf = \cos\theta \qquad 72$$

The real part of equation 70 is the surface resistance, and is given by

$$r = \frac{16}{3\pi\sigma\delta}\left[1-\left(1-\frac{d^2}{\delta^2}\right)^{3/2}\right] \qquad 73$$

hence the loss per unit area, from equation 67 is

$$N = \frac{8H_o^2}{3\pi\sigma\delta}\left[1-\left(1-\frac{d^2}{\delta^2}\right)^{3/2}\right] \qquad 74$$

For the case when the half thickness is greater than the depth of penetration, the solution is given by equation 38.

By comparison of equation 74 with equation 38, it is seen that the loss is independent of d as long as d is greater than δ. Hence the maximum value of d/δ to be used in equation 74 is unity.

Extensive experimental work was performed to substantiate the derived formulae.

The predicted waveforms shown in Figure 7 are compared with the wave forms of search coil voltages, with close correlation.

The best value of B_o, the saturation flux density, to be used is found to be 3/4 B_m where B_m is the flux density corresponding to H_o, the peak value of the mmf impressed at the surface. This, of course, will vary from material to material; however, this value is satisfactory for most cases.

The power loss for solid iron and constant permeability is[9]

$$N_1 = \frac{1}{2}\left[\frac{\omega B_m/H_o}{2\sigma}\right]^{1/2} H_o^2 \qquad 75$$

For the rectangular curve, using $B_o = B_m$ the power loss by equation 38 is

$$N = \frac{8}{3\pi}\left(\frac{\omega B_m/H_o}{2\sigma}\right)^{1/2} H_o^2 = \frac{16}{3\pi} N_1 = 1.697 N_1 \qquad 76$$

Using $B_o = 3/4\ B_m$

$$N = 1.47\ N_1 \qquad 77$$

Since the actual curve lies between the linear and the rectangular case, the limits are defined by equations 75 and 77.

The popular formula derived by Rosenberg[5] when converted to the same units and notation of this paper, is

$$N_r = \frac{2}{3}\left(\frac{\omega B_m/H_o}{2\sigma}\right)^{1/2} H_o^2 = 1.333\ N_1 \qquad 78$$

Thus, even though Rosenberg's assumptions were numerous and obscure, the results closely approach those given by equation 77.

The effect of hysteresis is believed to be less than 4 or 5 per cent of the total losses, except for very low frequencies; hence all test values are compared with calculated values which neglect hysteresis.

The calculated losses are compared with measured losses, over a frequency range from 30 cps. to 2,000 cps.; these in turn are compared with the losses predicted by the theories of Dreyfus[10] and Rosenberg. The calculated values by the new theory are within 15 per cent except for low frequency and low applied mmf, whereas the Rosenberg and Dreyfus values have errors as high as 400 per cent.

V. DETERMINATION OF LOSSES USING COMPLEX PERMEABILITY

A mathematical approach[11] to the problem of varying permeability is afforded by the conception of a complex value of permeability. This is equivalent to assuming that the hysteresis loop is elliptical in shape.

The core is assumed to be very long, solid, and of cylindrical shape with the radius being a. Hence equation 6 applies; i.e.:

$$\frac{\partial^2 H}{\partial r^2} + \frac{1}{r}\frac{\partial H}{\partial r} - \sigma\frac{\partial B}{\partial t} = 0 \qquad 79$$

When the magnetic intensity is assumed to be varying sinusoidally with time, and the permeability is assumed independent of time, equation 6 may be written

$$\frac{\partial^2 \dot{H}}{\partial r^2} + \frac{1}{r}\frac{\partial \dot{H}}{\partial r} - j\sigma\mu\omega\dot{H} = 0 \qquad 80$$

where the dot above a variable indicates a sinusoidal time variation. Hence at the surface of the material

$$\dot{H} = \dot{H}_o = H_o e^{j\omega t} \qquad 81$$

For purposes of convenience, the permeability is defined

$$\mu = \mu_o e^{-j\theta} \qquad 82$$

where μ_o and θ are constants. When the permeability is defined as in equation 82, even though it is the ratio of the flux density to

the magnetic intensity, it is by no means a constant. The significance of this definition will be discussed later.

Combining equation 80 and equation 82 gives

$$\frac{d^2\dot{H}}{dr^2} + \frac{1}{r}\frac{d\dot{H}}{dr} - j\sigma w \mu_o e^{-j\theta}\dot{H} = 0 \qquad 83$$

letting

$$z^2 = -j\sigma w \mu_o a^2 e^{-j\theta}$$

or

$$z^2 = \sigma w \mu_o a^2 e^{-j(\pi/2+\theta)} \qquad 84$$

equation 83 becomes

$$\frac{d^2\dot{H}}{dr^2} + \frac{1}{r}\frac{d\dot{H}}{dr} + \frac{z^2}{a^2}\dot{H} = 0 \qquad 85$$

This general solution of this equation is

$$\dot{H} = A J_o\left(\frac{zr}{a}\right) + B Y_o\left(\frac{zr}{a}\right)$$

where A and B are constants, and J_o and Y_o are Bessel functions of zero order and of the first and second kinds respectively. Since Y_o (0) is equal to infinity from a physical consideration, B must be zero. Thus, letting $H = H_o$ at the surface where $r = a$,

$$\dot{H} = \dot{H}_o \frac{J_o(zr/a)}{J_o(z)} \qquad 86$$

The total flux within the core, is obtained by integrating the flux density over the cross section of the core, thus for constant permeability

$$\dot{\phi} = 2\pi \mu_o e^{-j\theta} \int_0^a r \dot{H} \, dr \qquad 87$$

thus

$$\dot{\phi} = 2\pi \mu_o e^{-j\theta} \dot{H}_o \frac{a^2 J_{1(z)}}{z J_{o(z)}} \qquad 88$$

The penetration function is now defined as the ratio which the maximum value of the mean flux density within the core bears to the maximum flux density of the surface. Hence calling P the penetration function, we have

$$P = \frac{1}{\pi a^2} \left| \frac{\dot{\phi}}{\mu_o e^{-j\theta} \dot{H}_o} \right| \qquad 89$$

or from equation 88

$$P_{(z)} = \frac{2}{|z|} \left| \frac{J_{1(z)}}{J_{o(z)}} \right| \qquad 90$$

The penetration function is plotted for several values of θ in Figure 13.

The power per unit of length can be found directly from equation 86 and 88, calling this loss W, we get

$$W = Re \left[\dot{H}_o \frac{\partial \dot{\phi}}{\partial t} \right] \qquad 91$$

or

$$W = Re \left\{ \left[-\pi \omega \mu_o a^2 e^{-j(\pi/2 + \theta)} \right] \frac{H_{rms}^2 J_{1(z)}}{z J_{o(z)}} \right\} \qquad 92$$

where H_{rms} is the root-mean-square value of H_o, noting that

$$\omega \mu_0 a^2 e^{-j\left(\pi/2 + \theta\right)} = \frac{z^2}{\sigma} \qquad 93$$

we have

$$W = Re\left[-\frac{\pi z H^2_{rms}}{\sigma} \cdot \frac{J_{1(z)}}{J_{0(z)}}\right] \qquad 94$$

It is, in general, of more interest to consider the loss per unit volume, W_v. Hence

$$W_v = \frac{W}{\pi a^2} \qquad 95$$

or from equation 92

$$W_v = \omega \mu_0 H^2_{rms} L_{(z)} \qquad 96$$

where

$$L_{(z)} = Re\left\{\left(e^{j\left(\pi/2 - \theta\right)}\right) \frac{J_{1(z)}}{z J_{0(z)}}\right\} \qquad 97$$

The loss function, $L_{(z)}$, is plotted in Figure 14 for various values of θ.

The solution for the problem when the permeability varies across the section of the core is much more complicated. Equation 1 can, in general, be solved by a power series expansion. However, it is not likely that a simple solution will result, but there is a group of variable permeability distributions which are susceptible to ready solution. These will now be considered and the significance which may be attached to them will be discussed later.

Retaining the concept of complex permeability, assume

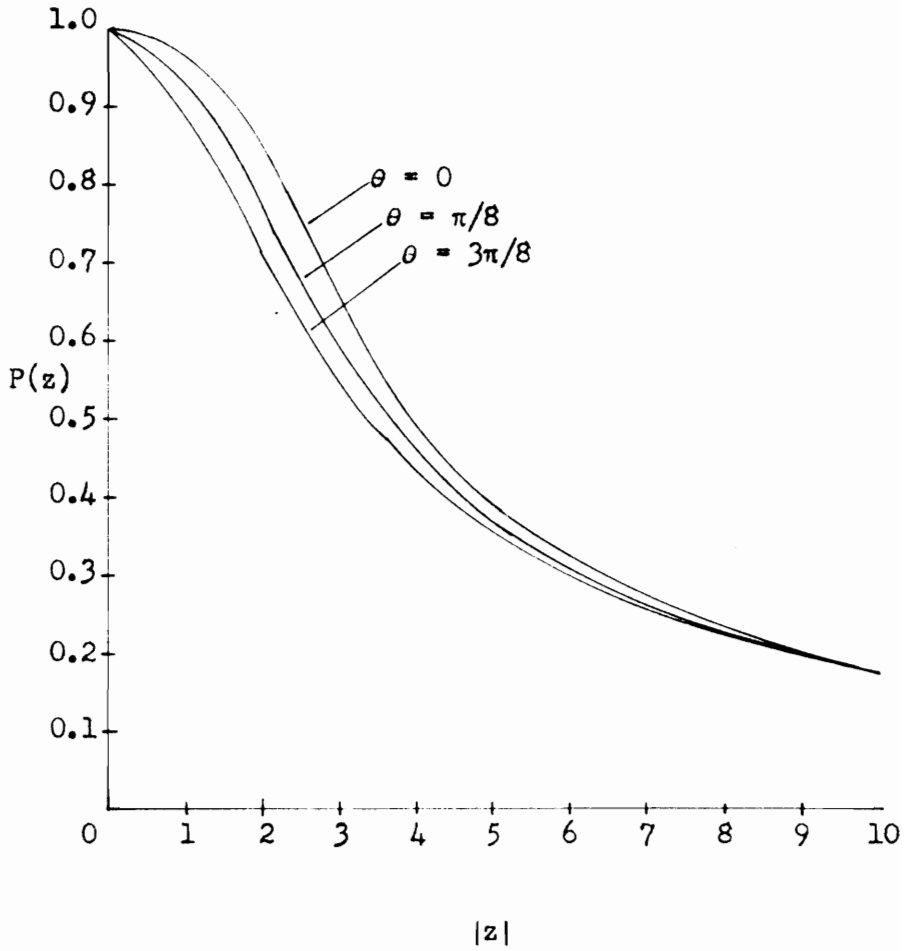

Figure 13 The penetration function

$$\mu = \mu_0 e^{-j\theta}\left(\frac{r}{a}\right)^P \qquad 98$$

Hence, equation 83 becomes

$$\frac{d^2\dot{H}}{dr^2} + \frac{1}{r}\frac{d\dot{H}}{dr} - j\sigma\omega\mu_0 e^{-j\theta}\left(\frac{r}{a}\right)^P \dot{H} = 0 \qquad 100$$

Letting

$$z^2 = \left(\frac{2}{2+p}\right)^2 \sigma\omega\mu_0 a^{2-p} e^{-j(\pi/2+\theta)} \qquad 101$$

Equation 100 becomes

$$\frac{d^2\dot{H}}{dr^2} + \frac{1}{r}\frac{d\dot{H}}{dr} + \left(\frac{2+p}{2}\right)^2\left(\frac{z}{a}\right)^2 r^p \dot{H} = 0 \qquad 102$$

Defining a new variable

$$\eta = r^{1+\frac{p}{2}} \qquad 103$$

equation 102 becomes

$$\frac{d^2\dot{H}}{d\eta^2} + \frac{1}{\eta}\frac{d\dot{H}}{d\eta} + \frac{z^2}{a^2}\dot{H} = 0 \qquad 104$$

which is similar to equation 85, so has a similar solution. However, since at the surface $\eta = a^{1+\frac{p}{2}}$, the solution is

$$\dot{H} = \dot{H}_0 \frac{J_0(zr/a)}{J_0(za^{p/2})} \qquad 105$$

The total flux density is obtained by integrating the flux density over the cross section of core. Thus

$$\dot{\phi} = 2\pi\mu_0 e^{-j\theta}\int_0^a r\left(\frac{r}{a}\right)^P \dot{H}\, dr \qquad 106$$

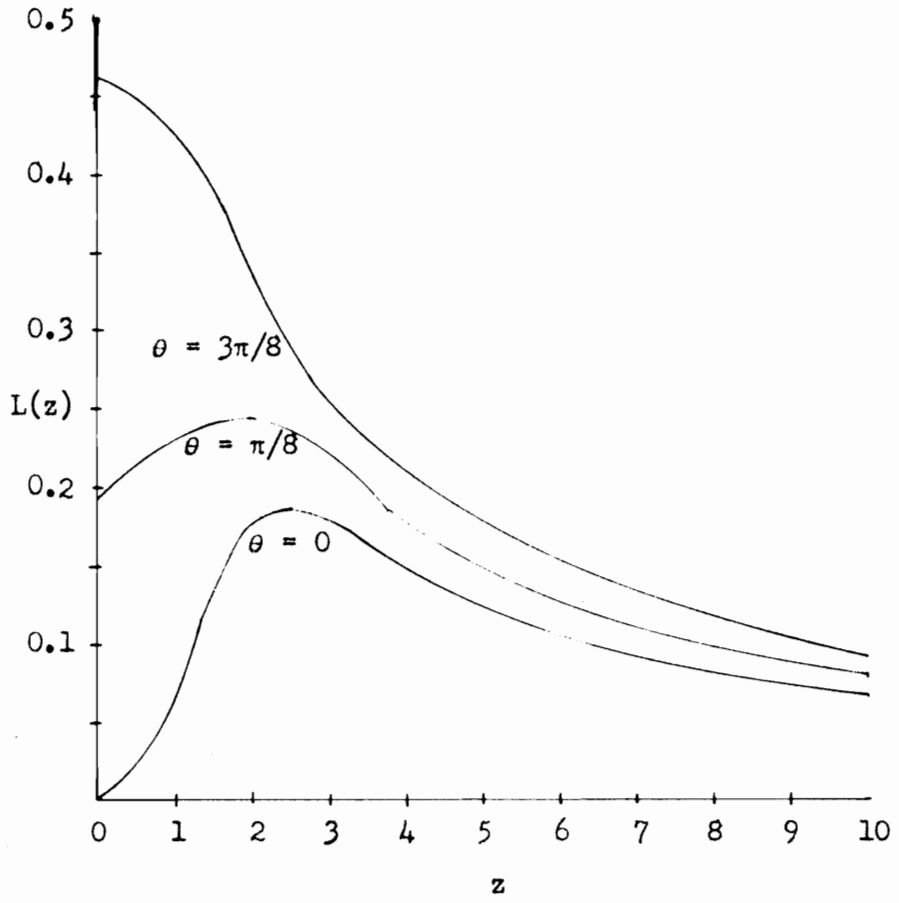

Figure 14 The loss function

or

$$\dot{\phi} = 2\pi\left(\frac{2}{2+\rho}\right)\frac{\mu_0 e^{-j\theta}}{a^{\rho}}\int_0^{a^{1+\frac{\rho}{2}}} \eta \dot{H}\, d\eta \qquad 107$$

Combining equations 105 and 107, we get

$$\dot{\phi} = 2\pi\left(\frac{2}{2+\rho}\right)\frac{\mu_0 \dot{H}_0 e^{-j\theta}}{a^{\rho} J_0(z a^{\rho/2})}\int_0^{a^{1+\frac{\rho}{2}}} \eta\, J_0(z\eta/a)\, d\eta \qquad 108$$

Evaluating this integral leads to the expression

$$\dot{\phi} = 2\pi\left(\frac{2}{2+\rho}\right)\frac{\mu_0 \dot{H}_0 e^{-j\theta} J_1(z a^{\rho/2})}{\left(a^{\frac{\rho}{2}-2}\right) z\, J_0(z a^{\rho/2})} \qquad 109$$

The average power per unit of length is found by equation 91, thus

$$W = Re\left[\left(\frac{4\pi\omega\mu_0}{2+\rho} a^{2-\frac{\rho}{2}}\right)\left(e^{j(\pi/2+\theta)}\right)\left(\frac{H^2_{rms}\, J_1(z a^{\rho/2})}{z\, J_0(z a^{\rho/2})}\right)\right] \qquad 110$$

Hence, the loss per unit volume is

$$W_v = \frac{W}{\pi a^2} = 2\omega\mu_0 H^2_{rms}\left(\frac{2}{2+\rho}\right)\left[Re\left\{e^{j(\pi/2-\theta)}\,\frac{J_1(z a^{\rho/2})}{z a^{\rho/2} J_0(z a^{\rho/2})}\right\}\right] \qquad 111$$

This reduces to

$$W_v = 2\omega\mu_0 H^2_{rms}\left(\frac{2}{2+\rho}\right) L_{(z a^{\rho/2})} \qquad 112$$

Where L is the same loss function as shown in Figure 14, it may be convenient to remove the factor p and replace it in an appropriate manner by the mean permeability

$$\mu_m e^{-j\theta} \qquad 113$$

The mean permeability is given by

$$\mu_m e^{-j\theta} = \frac{2}{a^2}\int_0^a \mu\, r\, dr$$

$$= \frac{2\mu_0 e^{-j\theta}}{a^{2+P}}\int_0^a r^{1+P}\, dr \qquad 114$$

From equations 112 and 114, we have

$$W_v = 2\pi w H^2_{rms}\, \mu_m\, L\, (2a^{P/2}) \qquad 115$$

In this case, from equation 101 we get

$$2a^{P/2} = \left(\frac{2a}{2+P}\right)(\sigma w \mu_0)^{1/2}\, e^{j(3\pi/4 - \theta/2)} \qquad 116$$

hence, from equation 114, equation 116 becomes

$$2a^{P/2} = \mu_m a \left(\frac{\sigma w}{\mu_0}\right)^{1/2} e^{j(3\pi/4 - \theta/2)} \qquad 117$$

To consider the significance of the above solutions, it is noted that in the case of sinusoidal variations of the magnetic intensity, the assumption of a constant complex value of permeability suggests a fixed angular displacement between the flux density and the magnetic intensity. By assuming constant complex permeability the following equations may be written:

$$H = H_0 \sin wt \qquad 118$$

$$B = B_m \sin(\omega t - \theta) \qquad 119$$

By eliminating wt from equations 118 and 119, the relation between the flux density and the magnetic intensity is an ellipse as shown in Figure 15.

It may be shown that

$$b \approx \mu_0 H_0$$

$$c \approx H_0 \sin\theta \qquad 120$$

It is apparent that the shape of the loop is independent of frequency.

The area of the ellipse can be approximated by

$$\pi bc \approx \pi \mu_0 H_0^2 \sin\theta \qquad 121$$

Since the maximum flux density is the product of the maximum permeability and the maximum magnetic intensity, the area is proportioned to

$$B_m^2 \frac{\sin\theta}{\mu_0} \qquad 122$$

By considering θ and μ_0 as constants we are simulating the core where the area of the loop is proportioned to the square of the flux density. To simulate hysteresis loss the area of the loop has to be independent of frequency and has to be proportional to a power of the maximum flux density of the order of 1.6.

An actual hysteresis loop has the form shown in Figure 16.

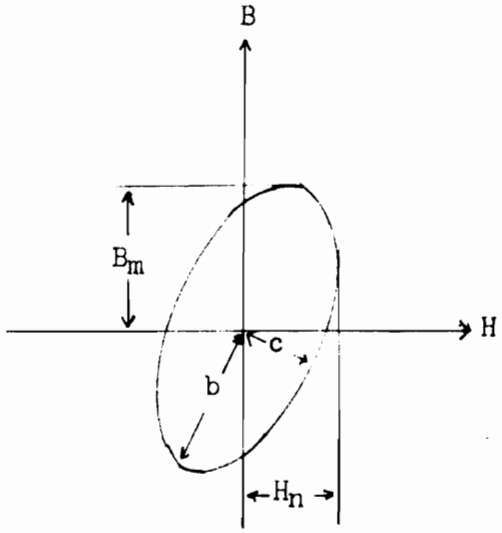

Figure 15 Elliptical B-H relationship

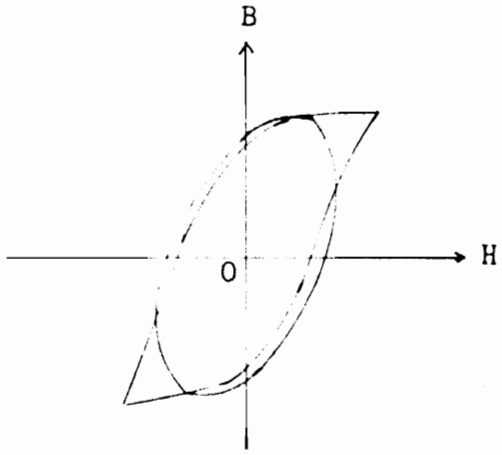

Figure 16 Hysteresis loop and equivalent ellipse

Harmonics in the flux density and magnetic intensity waveforms are produced due to the irregular shape of the hysteresis loop, but these are ignored in the present treatment. The best choice of θ and μ_o for a given hysteresis loop is one which yields an ellipse which has the same area and angle. Figure 16 shows and ellipse which has the same area and angle as the actual hysteresis loop. From equation 116, if A is the area of the hysteresis loop, then μ_o is chosen so that its value is

$$\mu_o = \frac{\pi B_m^2 \sin\theta}{A} \qquad 123$$

By this method of analysis the combined effects of eddy-current and hysteresis loss may be considered. In Figure 13 the curve for θ equal zero corresponds to the case where the hysteresis loop may be represented as a straight line, whereas the other curves apply to cases where hysteresis loss is present. It will be noted that the amount of penetration is very much the same whether hysteresis is present or not.

The assumption of uniform permeability, even though the core is homogeneous in character, cannot always be justified. When the core is subjected to magnetization the induced eddy-currents have a shielding effect, hence the fields within the core may not be as expected. It is well known that a magnetic material has a smaller effective permeability at a low flux density than at a high flux density. Therefore, for a given material, there will be a definite relation between the effective permeability and the range

of change of the magnetic intensity. Let us consider the problem in which we are given a definite relation as above and are to determine the magnetization loss for a given frequency and for a given applied magnetizing field. These given conditions will determine how the magnetic intensity decreases from the surface to the center of the core. The main assumption made is that this decrease can be represented by a value of permeability given by equation 98. The value of the factor p determines the shape of the permeability versus magnetic intensity curve, the problem is to determine the particular value of this factor which best suits the form of the actual curve.

Using the same terminology as before, equation 105 gives the relation between the magnetic intensity and r. The values of radius, conductivity, frequency and the range of the maximum magnetic intensity having been selected, the values of μ_o and θ are determined. Assuming θ to be constant, equation 117 enables us to calculate k, where

$$2a^{p/2} = \frac{\mu_m}{\mu_o} k \qquad 124$$

Also from equation 114

$$1 + \frac{p}{2} = \frac{\mu_o}{\mu_m} \qquad 125$$

Combining equations 105, 124 and 125, we get

$$\frac{H}{H_o} = \frac{J_o\left[\frac{\mu_m}{\mu_o} k \left(\frac{r}{a}\right)^{\mu_o/\mu_m}\right]}{J_o\left[\frac{\mu_m}{\mu_o} k\right]} \qquad 126$$

Finally, using equations 98 and 125, we get

$$\frac{\dot{H}}{\dot{H}_0} = \frac{J_0\left[\frac{\mu_m}{\mu_0} k \left(\frac{\mu}{\mu_0}\right)^{\frac{\mu_0}{2(\mu_0-\mu_m)}}\right]}{J_0\left[\frac{\mu_m}{\mu_0} k\right]} \qquad 127$$

Figure 17 shows this relationship for the case where k equals 5 and θ is 45 degrees. These curves then must be compared with the known effective permeability and magnetic intensity relation and the appropriate value of the mean permeability can be deduced.

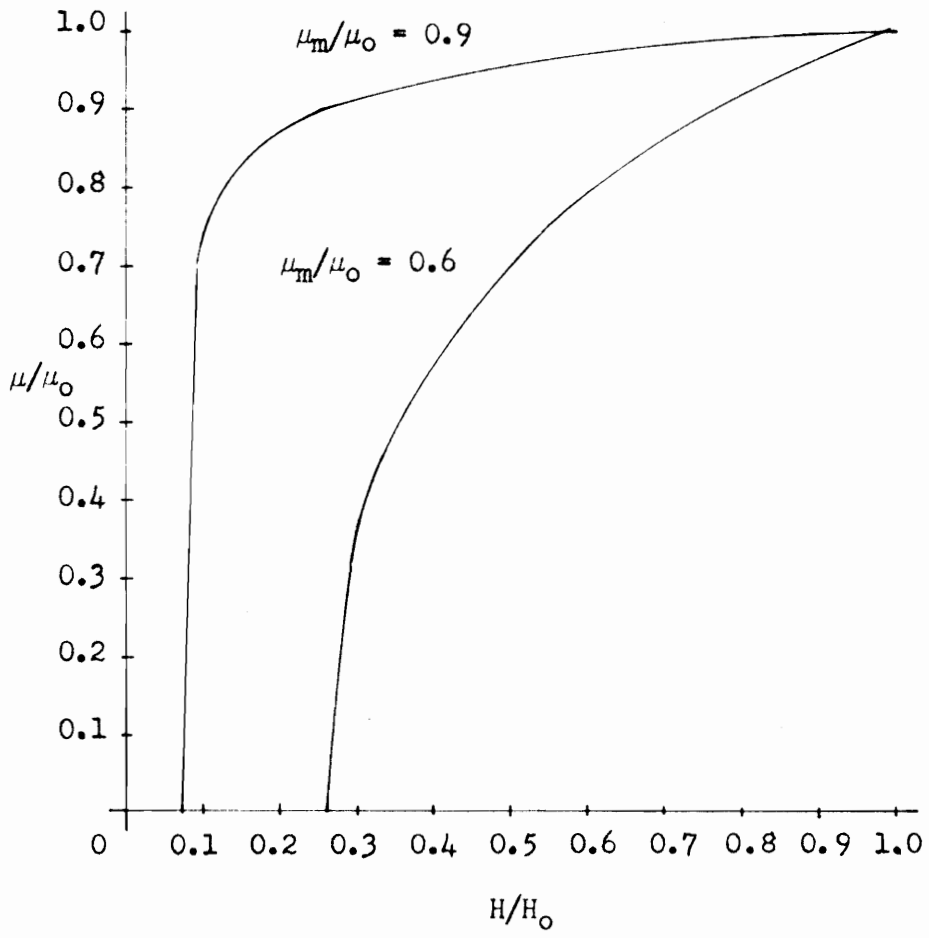

Figure 17 μ—H relationships for variable permeability

VI. GRAPHICAL DETERMINATION OF IRON LOSSES

A method[12] of considerable interest is a graphical construction of the flux and magnetic intensity curves.

Consider an infinite half-space of solid iron with its surface on the y, z-plane and excited so that the magnetizing force at the surface is in the y-direction only. The x-direction is normal to the y, z-plane and is measured towards the surface. Hence, at any point (x,y,z), H_y, B_y ϕ_y, alone exists, as a function of x only. In what follows the subscript is dropped and the above quantities are denoted by H, B and ϕ respectively.

By assuming constant permeability and neglecting hysteresis, the effects at depth x produced by the surface magnetizing force,

$$H = H_0 \sin \omega t \qquad 128$$

may be determined.

Maxwell's equations are

$$\bar{\nabla} \times \bar{h} = \sigma \bar{e} \qquad 129$$

and

$$\bar{\nabla} \times \bar{e} = -\frac{\partial}{\partial t} \bar{b} \qquad 130$$

Considering the above geometry, equations 129 and 130 reduce to

$$\frac{\partial H}{\partial x} = \sigma E \qquad 131$$

and

$$\frac{\partial E}{\partial x} = -\frac{\partial}{\partial t} B \qquad 132$$

Combining equations 131 and 132 and eliminating E, we get

$$\frac{\partial^2 H}{\partial x^2} = \sigma \frac{\partial B}{\partial t} \qquad 133$$

which, for constant permeability and a sinusoidal variation of magnetic intensity at the surface, becomes

$$\frac{d^2 \dot{H}}{dx^2} - j\omega\mu\sigma\dot{H} = 0 \qquad 134$$

Solving equation 134 for the given boundary condition yields

$$\dot{H} = H_o e^{-mx} \cos(\omega t - mx) \qquad 135$$

where

$$m^2 = \omega\mu\sigma \qquad 136$$

Similarly

$$\dot{B} = B_m e^{-mx} \cos(\omega t - mx) \qquad 137$$

also

$$\dot{\phi} = \phi_m e^{-mx} \cos(\omega t - mx - \pi/4) \qquad 138$$

where

$$\phi_m = \frac{\mu H_o}{\sqrt{2}\, m} \qquad 139$$

These equations show that the H-vector leads the ϕ-vector by a constant angle of 45 degrees. The above solution is for the case of constant permeability, which is in general true for the lower part of the B-H curve. For the portion near the knee of the curve a graphical construction is used.

Pohl[13] has developed a graphical method to determine the flux and current distribution in solid iron under saturation. The values of H and ϕ are assumed to be known at an arbitrary value of x. The problem is then one of determining the values of $H + \Delta H$ and $\phi + \Delta\phi$ at an adjacent layer at the distance $x + \Delta x$. From the magnetic intensity versus flux density curve and the assumed value of H, the value of B is determined. From the assumed flux ϕ, E_z the electric field intensity is found, hence $\Delta H = \sigma E_z \Delta x$ is determined. Lastly, $\Delta\phi$ is given by $B\Delta x$. These quantities are added vectorially to give their magnitude and phase at $x + \Delta x$. The starting point is where the linearity of the B-H curve terminates. This step by step construction is illustrated in Figure 18.

An effort to make the graphical construction independent of the flux density, angular frequency and resistivity is based on the following considerations:

1. The magnetization curve is approximated as shown in Figure 19. This implies that the flux density, B_s, at any layer is independent of the magnetizing force at that layer.

2. The vector quantities ΔH and $\Delta\phi$ would now be

$\Delta H = \phi \sigma \omega \Delta x$

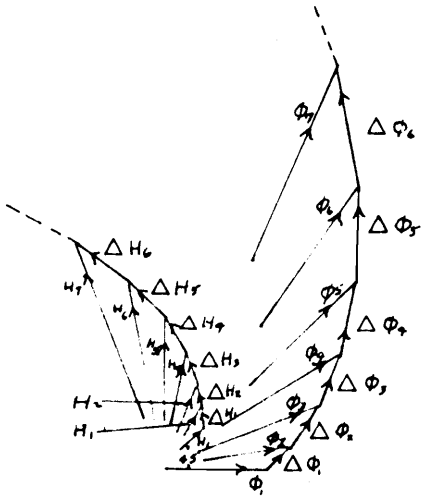

Figure 18 Step-by-step graphical construction

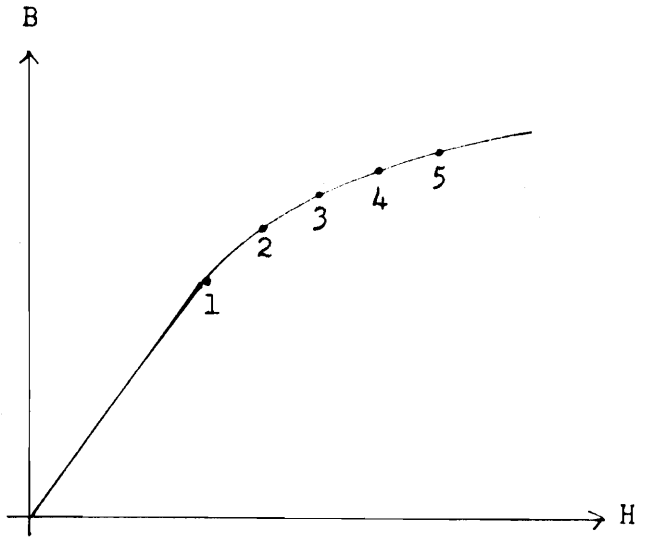

Figure 19 Saturation curve used for the step-by-step analysis

$$\Delta \phi = B_s \Delta x \qquad 141$$

Suppose that the ϕ and H-loci have been drawn for $B_s = B_{so}$ and $\omega\sigma = 1$. In general the initial value of H will be finite and that for ϕ will be zero. For this construction to apply for other values of B_s, say B_{s1}, and for other values of $\omega\sigma$, it is only necessary to note from equations 140 and 141 that the ϕ and H-loci will be magnified by scale factors B_{s1}/B_{so} and $\omega\sigma B_{s1}/B_{so}$ respectively. For example, if these two loci had been drawn for $B_{so} = 1$ weber per square meter and $\omega\sigma = 1$ and with initial values $H_1 = 1$ and $\phi_1 = 0$, then the same curve will apply for $B_{so} = 2$ webers per square meter and $\omega\sigma = 1/2$.

For the case of the infinite half space of iron, a table for the step by step construction is developed for a Δx of 0.001 centimeter.

An examination of the graphical construction for the ϕ and H-loci for any magnetization curve leads to certain interesting interpretations.

1. The tangent to the H-locus at any point is normal to the corresponding radius vector on the ϕ-locus.

2. The tangent of the ϕ-locus at any point is parallel to the corresponding radius vector of the H-locus.

3. From Figure 20 and equations 140 and 141,

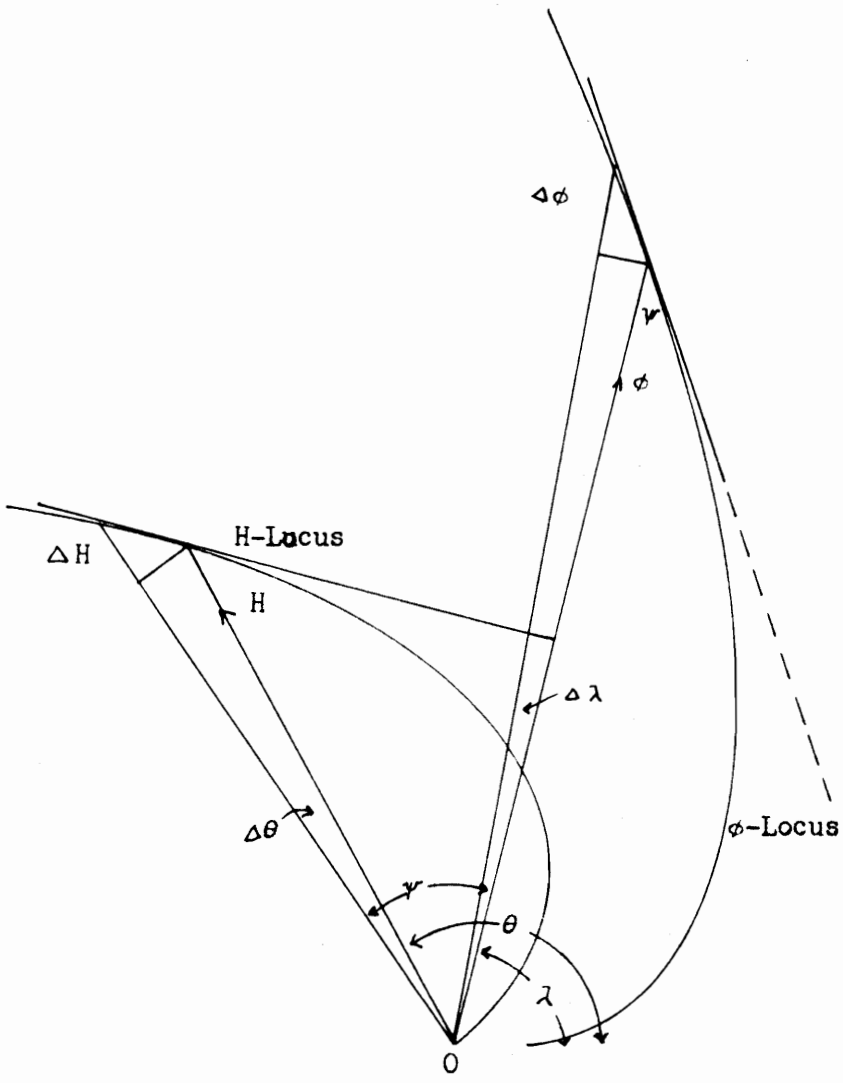

Figure 20 The geometry of ϕ- and H-loci

$$\frac{dH}{\sin\psi} = \sigma\omega\phi\,dx \qquad 142$$

Since the induced emf per unit axial length is $\omega\phi$, the current density is

$$\sigma\omega\phi \qquad 143$$

hence, the power loss in a layer of thickness x and unit width is

$$\frac{1}{2}ei\,dx = \frac{1}{2}\sigma\omega^2\phi^2\,dx \qquad 144$$

Therefore the total power loss per unit surface area is

$$\frac{1}{2}\int_0^x \sigma\omega^2\phi^2\,dx \qquad 145$$

From a physical consideration, the power loss is

$$\frac{1}{2}EH\sin\psi \qquad 146$$

Combining equations 146 and 142, the equation for the total power loss per unit surface area is found

$$\frac{1}{2}\frac{H}{\sigma}\frac{dH}{dx} \qquad 147$$

Equating equations 147 and 145 and differentiating, we get

$$\phi = \frac{1}{\sigma\omega}\left[H\frac{d^2H}{dx^2} + \left(\frac{dH}{dx}\right)^2\right]^{1/2} \qquad 148$$

which is the general expression for the flux below the surface at any layer at a depth x. Also from equations 142 and 148,

$$\sin\psi = \frac{\frac{dH}{dx}}{\left[H\frac{d^2H}{dx^2} + \left(\frac{dH}{dx}\right)^2\right]^{1/2}} \qquad 149$$

where $\sin\psi$ is the power factor at the layer x.

These results indicate that if the variation of the amplitude of H as a function of x is known, it is a simple matter to calculate ϕ, x and the loss at any layer whether the region is saturated or not.

VII. PROPOSED METHOD OF SOLUTION USING CONCENTRIC SHELLS

The geometry to be considered is a solid circular cylinder of infinite length and radius a. Hence, equation 6 applies and is repeated here for convenience.

$$\sigma \frac{\partial B}{\partial t} = \frac{\partial^2 H}{\partial r^2} + \frac{1}{r} \frac{\partial H}{\partial r} \qquad 150$$

Equation 150 is solved for three different relationships between the magnetic intensity and the flux density. The first case is for constant permeability, the second takes into account saturation without hysteresis and the third solution includes the effects of hysteresis. For the case of constant permeability equation 150 may be solved exactly, however the results are of little practical interest since no known magnetic material has this characteristic, except for very low levels of excitation. Conversely, cases two and three are of great practical interest. Hence, even though the solutions for the latter cases are approximate, and by no means general, the results bear a closer relationship to the actual physical problem. Illustrations of the three approximate flux density versus magnetic intensity curves are shown in Figures 21, 22 and 23. The actual relation is shown in Figure 24.

Solution for Constant Permeability

When the permeability may be considered a constant, as in Figure 21, equation 150 may be written

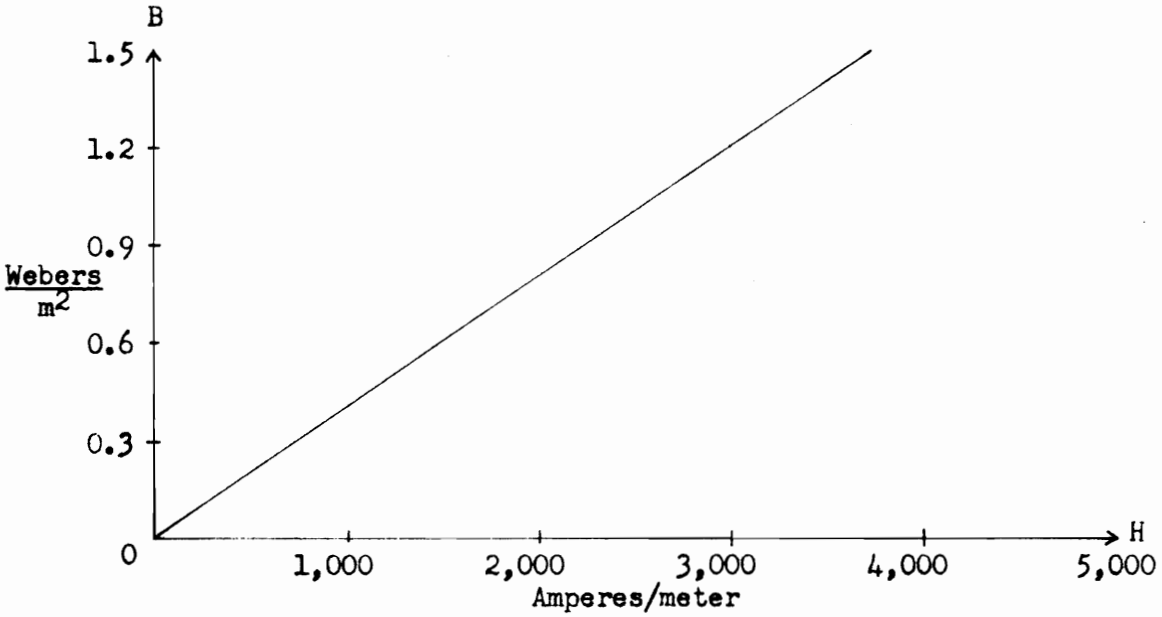

Figure 21 B-H relation for constant permeability

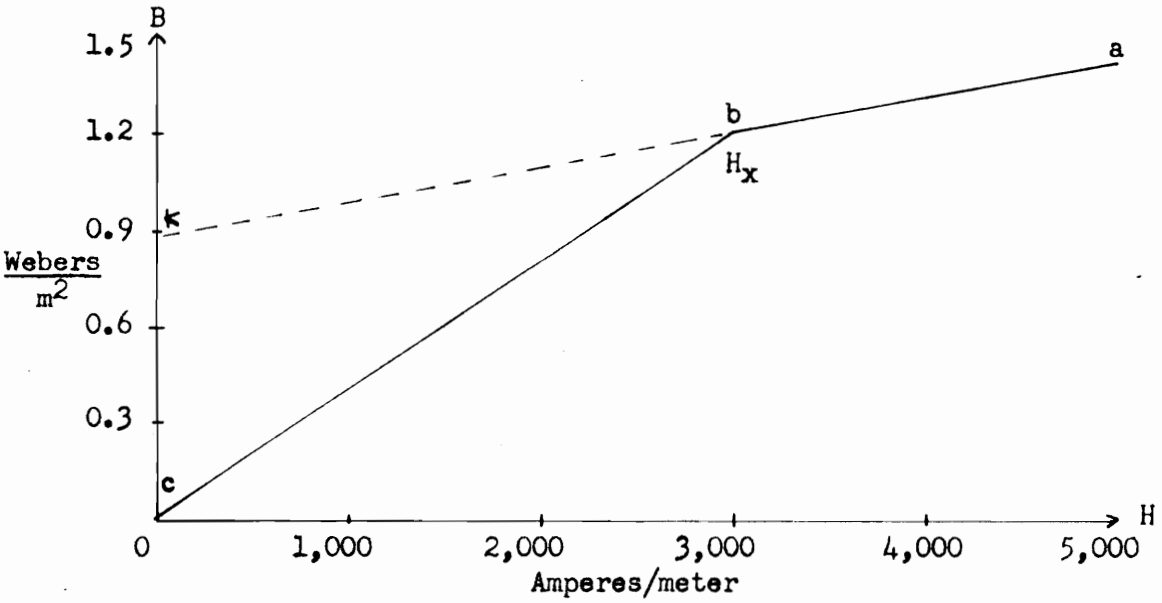

Figure 22 B-H relation where saturation is present

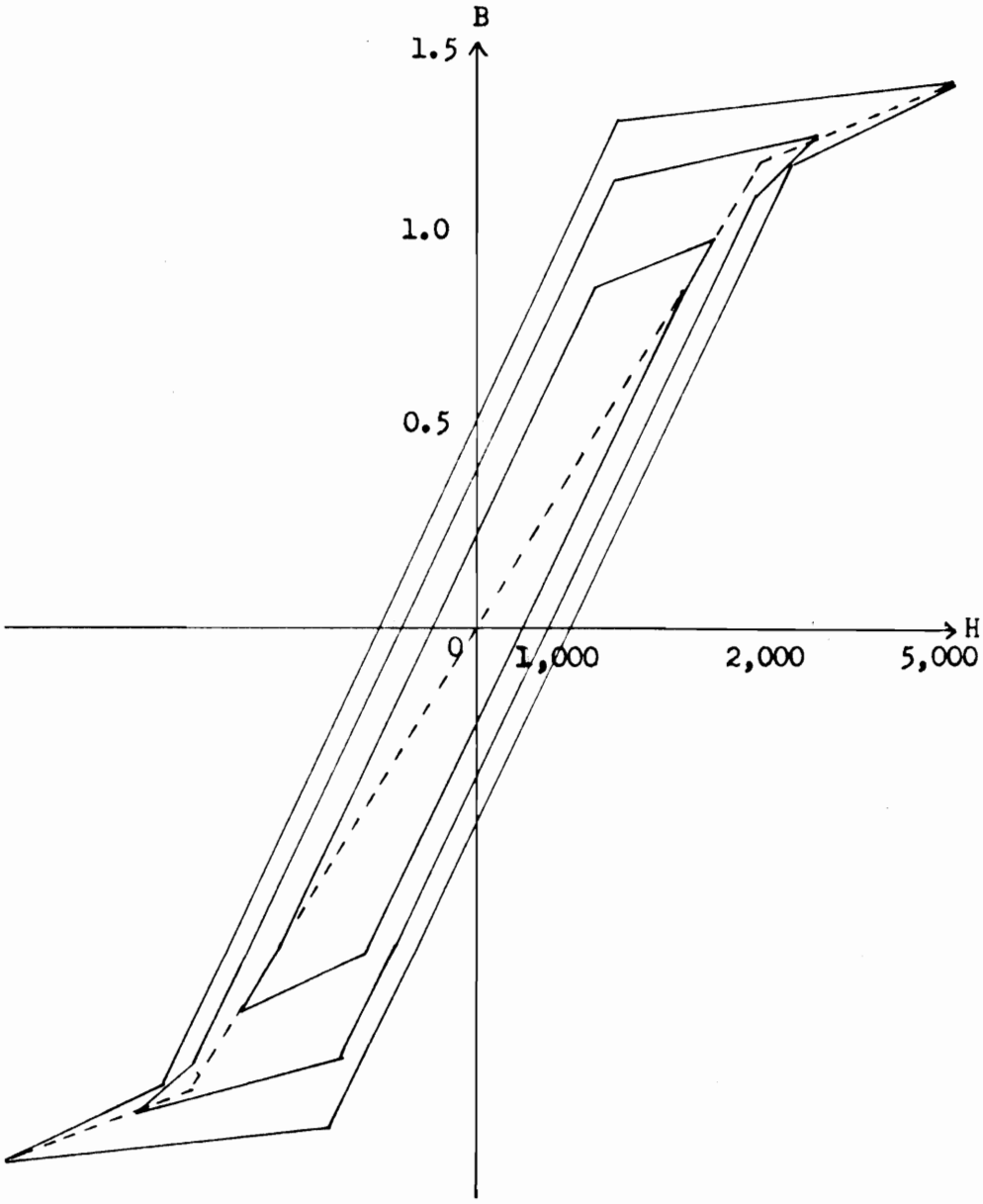

Figure 23 Approximate hysteresis curves

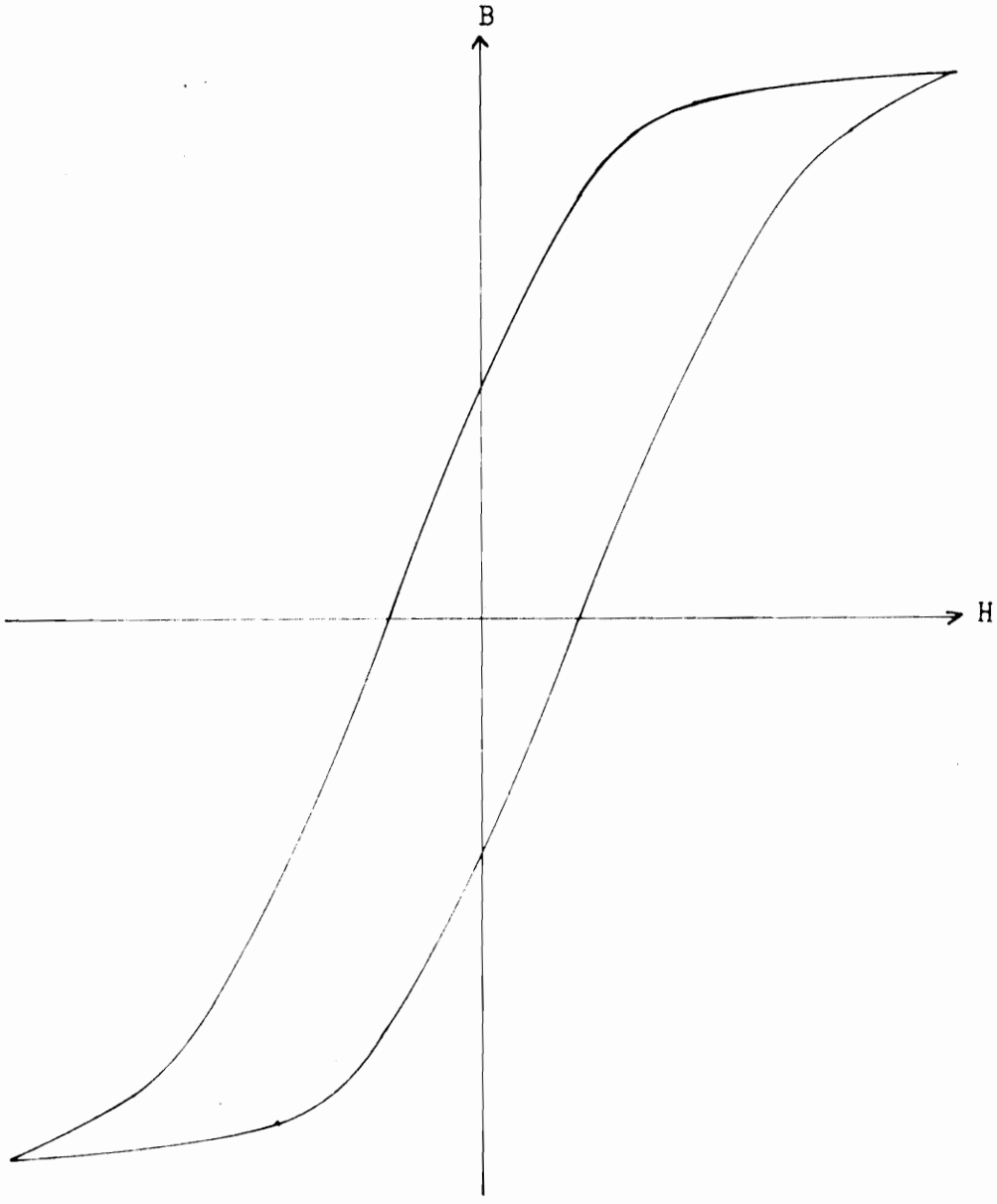

Figure 24 Actual hysteresis loop

$$\sigma \mu \frac{\partial H}{\partial t} = \frac{\partial^2 H}{\partial r^2} + \frac{1}{r} \frac{\partial H}{\partial r} \qquad 151$$

The excitation at the surface is a pure sinusoid of peak amplitude H_o, thus

$$\dot{H}_o = H_o e^{j\omega t} \qquad 152$$

and

$$\frac{\partial \dot{H}_o}{\partial t} = j\omega H_o e^{j\omega t} \qquad 153$$

Therefore equation 151 becomes

$$\frac{d^2 \dot{H}}{dr^2} + \frac{1}{r} \frac{d\dot{H}}{dr} - j\omega\sigma\mu\dot{H} = 0 \qquad 154$$

The general solution of equation 154 is

$$\dot{H} = A J_o(k r j^{3/2}) + B K_o(k r j^{3/2}) \qquad 155$$

where

$$k^2 = \sigma \omega \mu$$

J_o and K_o are Bessel functions of order zero and the first and second kind respectively. The coefficient B must be zero since K_o (0) has the physically impossible value of infinity. Considering the boundary condition given in equation 152, equation 155 becomes

$$\dot{H} = \dot{H}_o \frac{J_o(k r j^{3/2})}{J_o(k a j^{3/2})} \qquad 156$$

The distribution of the magnetic intensity with the radius is plotted in Figure 28. Where

$$\dot{H}_o = 5000 \cos 377t$$

$$\mu = 4 \times 10^{-4}$$

$$\sigma = 2 \times 10^{6}$$

Solution Using Approximate Saturation Curve

In cases where saturation is present, the previous solution is of little practical importance. To include the effects of saturation, the curve is approximated by two straight lines as shown in Figure 22. For the segment ab the relation between the magnetic intensity and flux density may be expressed as

$$B = mH + K \qquad 157$$

where m is the slope and K is the vertical ordinate intercept. The segment bc may be defined by

$$B = \mu H \qquad 158$$

where μ is the permeability. Since the portion of the curve we are on is determined by the instantaneous value of the magnetic intensity, equation 150 has two solutions. The constant K is independent of the instantaneous value of the magnetic intensity, hence equation 151, for the two regions defined by equations 157 and 158, becomes

$$\sigma m \frac{\partial H}{\partial t} = \frac{\partial^2 H}{\partial r^2} + \frac{1}{r}\frac{\partial H}{\partial r} \quad , H_k < \dot{H} < H_o \qquad 159$$

and

$$\sigma\mu \frac{\partial H}{\partial t} = \frac{\partial^2 H}{\partial r^2} + \frac{1}{r} \frac{\partial H}{\partial r} \quad , \quad 0 < \dot{H} < H_x \qquad 160$$

The magnetizing force as it penetrates in the iron is attenuated, hence if equations 159 and 160 are applied directly, the resulting solution would be true only if the magnetic characteristics of the material could be described as a family of curves in which the ratio of H_o to H_x is a constant. This, however, is not the case. The value of H_x remains constant independent of the peak value of H, hence as the magnetizing force moves into the iron, the amount of saturation becomes less and less, and eventually the magnetic intensity becomes less than H_x and equation 160 alone applies.

An approximate solution for this situation may be gotten by assuming for a thin shell that the ratio of H_o to H_x is a constant. At the inner surface a new peak value of the magnetic intensity exists. Using this new value of H, the equations are solved for the magnetic intensity at the inner surface of the next shell. This procedure is repeated until the center of the core is reached.

It is apparent that the magnetic intensity computed at the first inner surface will not have a purely sinusoidal waveform. The amount of distortion, however, is found to be small enough that the assumption of a purely sinusoidal waveform is reasonable. To include the effects of harmonics, the power dissipated in each shell is computed from the root-mean-square value of the actual waveform. The total power is the sum of the power found for each

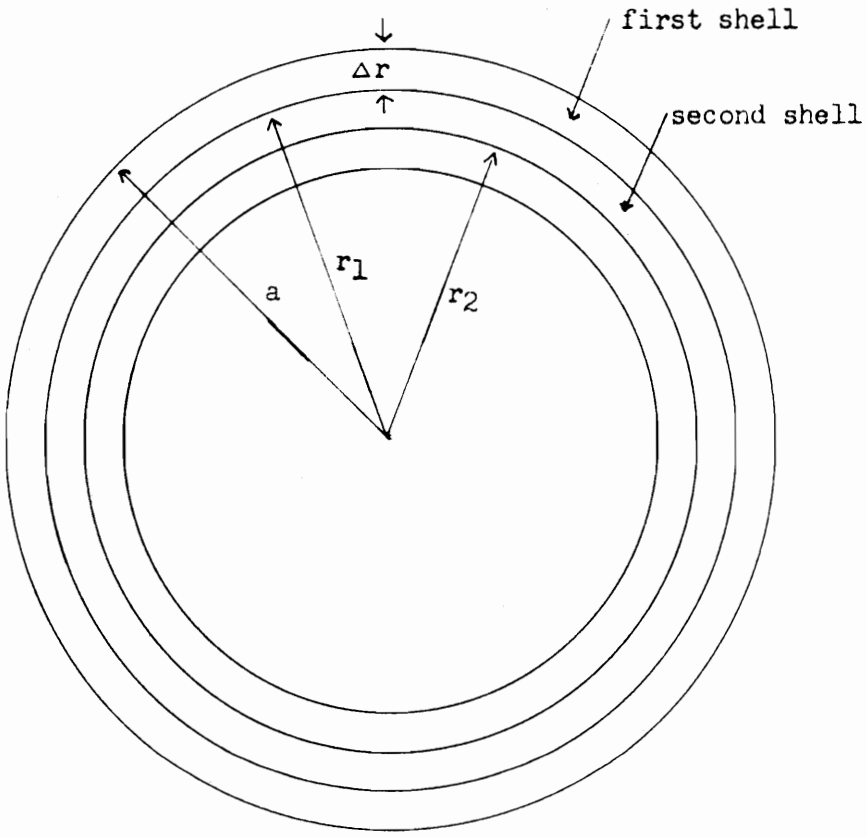

Figure 25 Solid cylinder approximated by concentric shells

shell.

For example, using Figure 22 and Figure 25, the solution of equation 159 for the first shell becomes

$$\dot{H} = 5000 \cos 377t \, \frac{J_0(k r_1 j^{3/2})}{J_0(k a_j^{3/2})} \qquad H_x < \dot{H} < H_0 \qquad 161$$

where

$$\sigma = 2 \times 10^6$$

$$m = 1 \times 10^{-4}$$

$$a = 1 \times 10^{-2}$$

$$\dot{H}_0 = 5000 \cos 377t$$

$$k^2 = m \omega \sigma$$

r_1 = radius of the core at the first inner surface

thus

$$\dot{H} = 5000 \cos 377t \, \frac{J_0(2.75 \times 10^2 r_1 j^{3/2})}{J_0(2.75 j^{3/2})} \qquad 162$$

letting

$$r_1 = .9a$$

we get

$$\dot{H} = 4370 \cos(377t - 11°) \qquad 163$$

Similarly, for equation 160 letting

$$k^2 = \sqrt{\mu \sigma \omega} = 5.5 \times 10^2$$

we get

$$\dot{H} = 3560 \cos(377t - 19°) \quad , \quad 0 < \dot{H} < H_x \qquad 164$$

The waveform resulting from equations 163 and 164 applied over the proper intervals of the period is shown in Figure 26. The root-mean-square of the waveform at the inner surface is computed from equations 163 and 164.

For the determination of the magnetic intensity at inner surface of the second shell, Figure 26 is approximated by a sinusoid with a peak amplitude given by the root-mean-square value of the magnetic intensity times the square root of two. The approximate waveform is shown by the dashed lines in Figure 26.

The value of the magnetic intensity for several values of radius and the power taken by each shell is shown in Table 1.

Solution Using Approximate Hysteresis Curve

The approximate hysteresis curve shown in Figure 23 is a closer representation of the actual relation between the magnetic intensity and the flux density than any of the previous curves. The method of analysis is the same as in the previous case except a completely new curve is followed when the peak amplitude of the magnetic intensity is changed. In other words, as the magnetic intensity diminishes as it goes into the iron, a family of nested curves is generated (Figure 23). The tips of the nested hysteresis curves given a locus of points from which the saturation curve used in the previous section is determined. In any given shell it

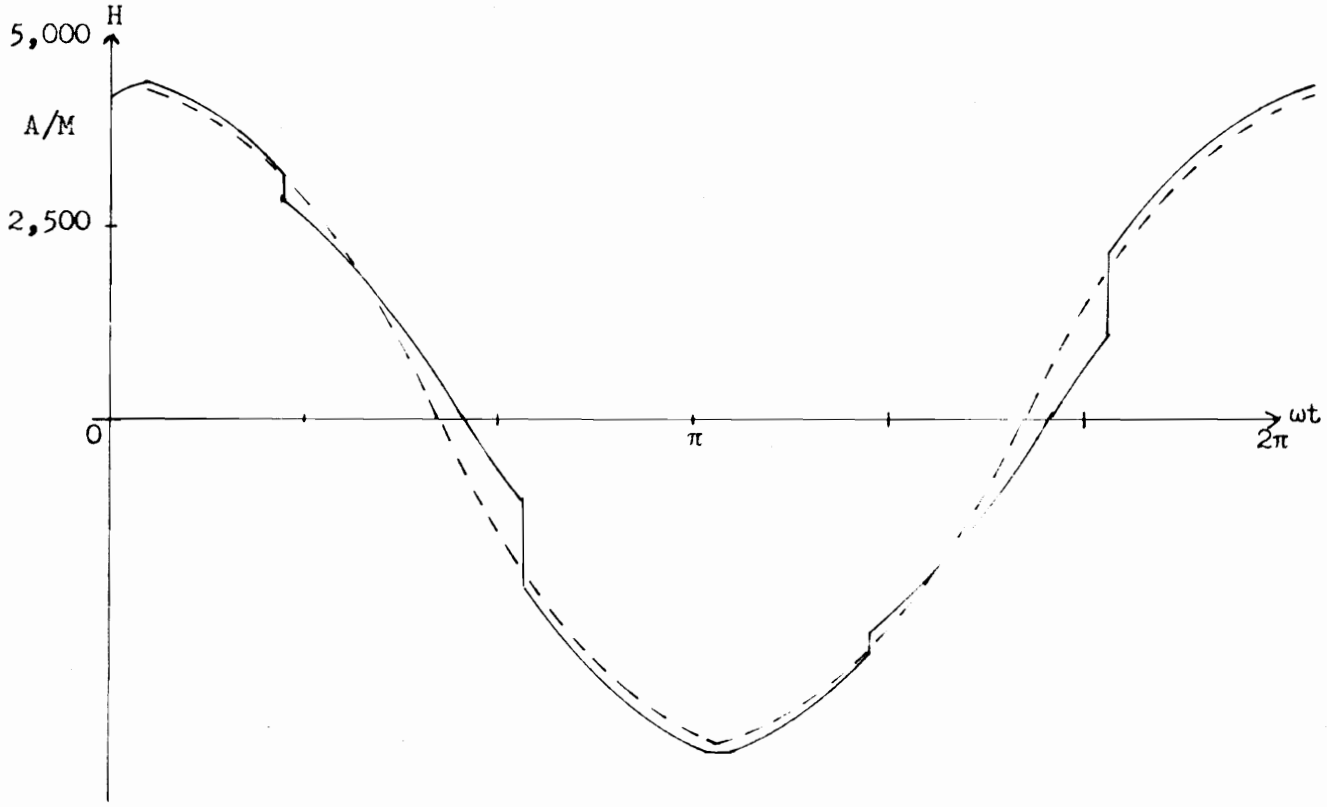

Figure 26 Actual magnetic intensity waveform at first inner surface and sinusoidal approximation used

is assumed that the appropriate loop at the surface of the shell applies through the entire shell.

Again the piece-wise method is used to determine the root-mean-square value of the magnetic intensity at the inner surface. As in the previous section, the resulting waveform is sufficiently sinusoidal so that for purposes of calculations in the next shell, a pure sinusoid of peak amplitude $\sqrt{2}\ H_{rms}$ may be assumed. The waveform at the first inner surface and its approximation is shown in Figure 27.

The result of a set of representative calculations is shown in Table 1.

Conclusions

The results of the representative calculation, tabulated in Table 2, are plotted in Figure 28. Inspection of Figure 28 reveals that without saturation the magnetic intensity decays quite rapidly as we move into the iron. The rate of decay becomes slower as saturation is introduced, and slower still when hysteresis is present. The significance of this may be realized by considering the Maxwell equation

$$\bar{\nabla} \times \bar{h} = \bar{j} = \sigma \bar{e}$$

which for the geometry considered reduces to

$$\frac{dH}{dr} = J$$

Hence the space rate of change of the magnetic intensity is equal

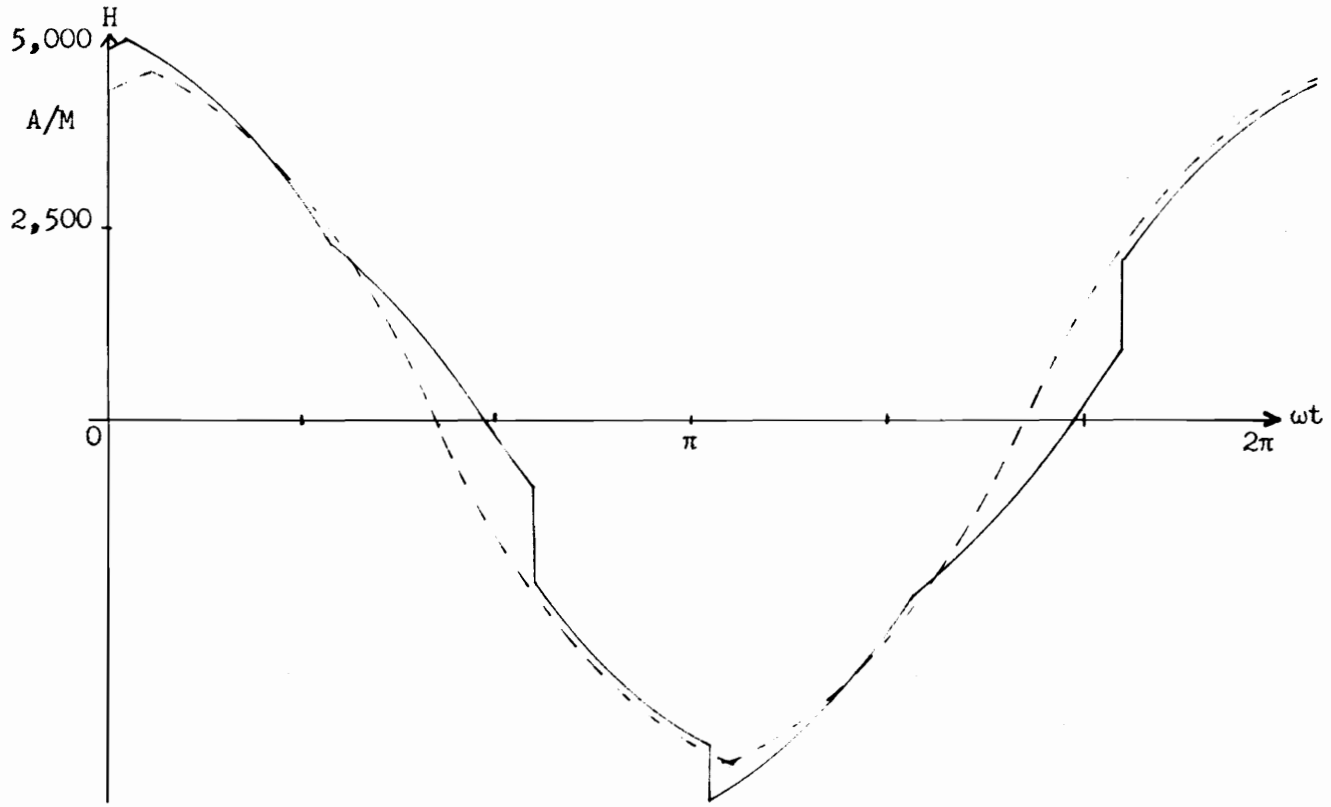

Figure 27 Actual magnetic intensity waveform at first inner surface and sinusoidal approximation when hysteresis is considered

TABLE I

MAXIMUM VALUE OF THE ASSUMED SINUSOID

AT EACH SHELL, FOR THE THREE CASES CONSIDERED

Radius	H_{linear}	$H_{hysteresis}$	$H_{saturation}$
$r = a$	5,000	5,000	5,000
$r_1 = .9a$	3,560	4,510	4,270
$r_2 = .8a$	2,580	4,010	3,700
$r_3 = .7a$	1,775	3,620	2,640
$r_4 = .6a$	1,360	3,250	1,940
$r_5 = .5a$	1,011	2,820	1,440
$r_6 = .35a$	707	2,350	1,005
$r_7 = .2a$	606	2,100	933
$r_8 = 0$	592	2,080	910

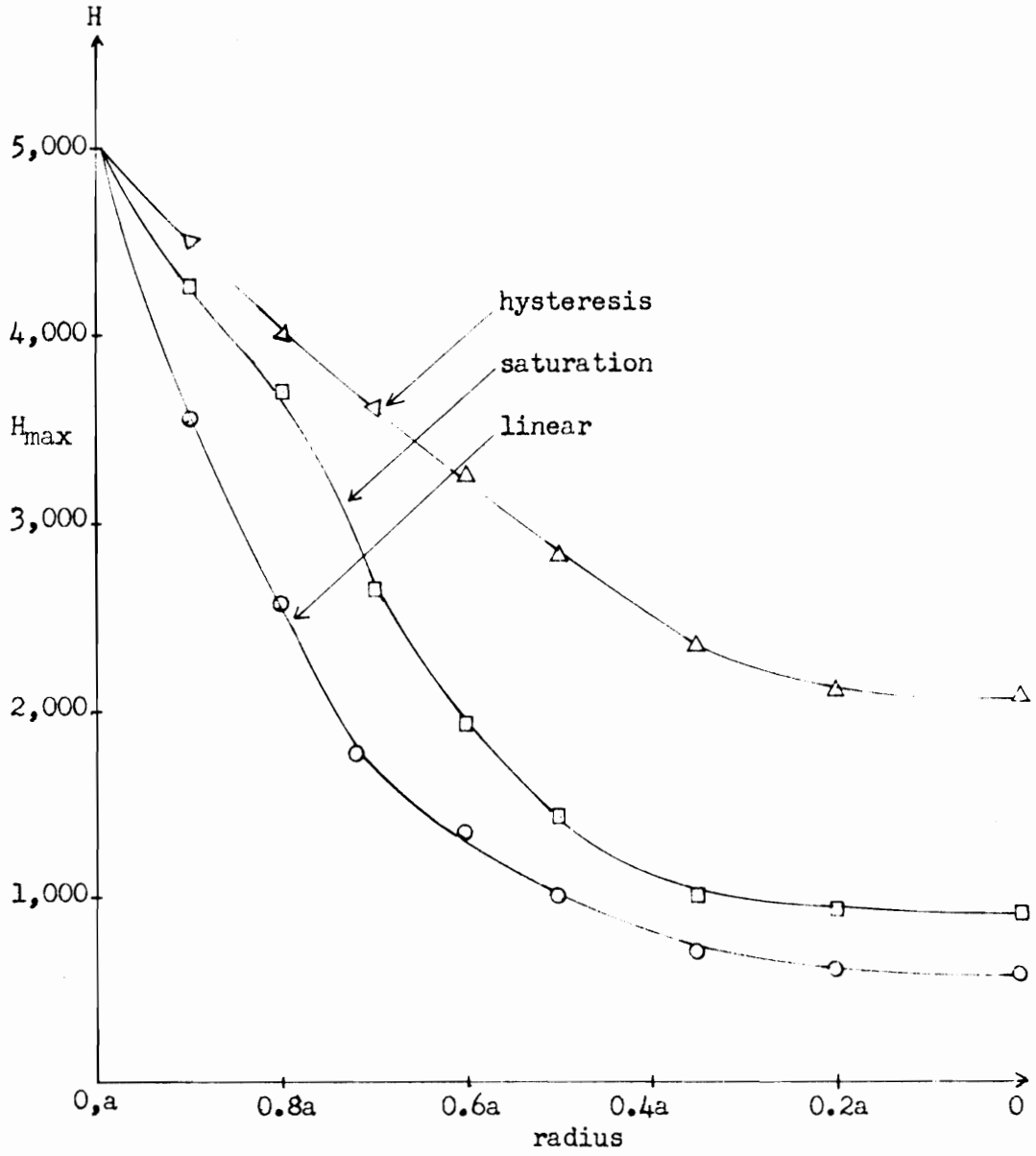

Figure 28 Maximum value of the magnetic intensity versus radius for the three cases considered

to the conduction current, which is nothing more than the slope of the curves being considered. Since the average power taken is proportional to the current density squared, it is apparent that the effect of saturation and hysteresis is to reduce the total power taken. Alternately, when saturation is present, the total flux produced, for a given exciting current, is less than that produced without saturation. Hence the eddy-current induced is less.

The above observations are made assuming a constant exciting current. The anomaly discussed earlier is based on the assumption of a constant flux density. If it is desired to determine the losses for a given flux density, equation 6 may be written in terms of flux density rather than magnetic intensity; i.e.:

$$\frac{\partial^2 H}{\partial r^2} + \frac{1}{r}\frac{\partial H}{\partial r} = \sigma \frac{\partial B}{\partial t}$$

where, in general

$$B = m H + K$$

or

$$H = \frac{B - K}{m}$$

For the case of saturation without hysteresis K and m are independent of the radius. Hence

$$\frac{\partial^2 B}{\partial r^2} + \frac{1}{r}\frac{\partial B}{\partial r} = m \sigma \frac{\partial B}{\partial t}$$

and the method of solution outlined before may be followed.

In the event hysteresis is present K and m will not be independent of the radius, hence the variation of these quantities will have to be determined from the family of curves used.

The sample calculations made were done by hand. If, however, thinner shells are taken to improve the accuracy of the approximation, it would be feasible to make the calculations using a digital computer.

VIII. REVIEW OF OTHER METHODS

Equation 6 is a non-linear, parabolic, partial differential equation. Methods for the numerical solution of partial differential equations have mainly been devised for specific problems. The methods so far developed have centered around the linear equations arising in physics and engineering, the heat equation, the wave equations and similar equations. Although some isolated non-linear equations have been solved, the general theory is still obscure.

Numerical methods tend to separate into two types. One the explicit type, where the numerical solution can be calculated step by step from the given differential equation and the known initial and boundary conditions. The other, the implicit type, where the unknown values are bound together by a set of simultaneous equations. The parabolic differential equation is of the explicit type.

The equation in question may be approximated[14] by a finite difference equation based on the point pattern shown,

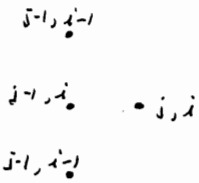

where the values are known for the nodes on the left, either from boundary conditions or from previous calculations. Hence, a typical

node (i,j) may be found by the following equation:

$$B_{i,j} = B_{i,j-1} + \frac{\Delta t}{\sigma(\Delta r)^2}\left[H_{i-1,j-1} - 2H_{i,j-1} + H_{i+1,j-1}\right] + \frac{\Delta t}{r_i \sigma \Delta r}\left[H_{i-1,j-1} - H_{i,j-1}\right]$$

where r_i is the radial coordinate of the node under consideration.

The ratio of Δt to Δr is of critical importance. If this ratio is either too large or too small, a large error will result. In fact, it may be that the solution is not stable.

A great deal of effort was expended in an attempt to solve equation 6 by this method using an IBM 650 computer. The major problem encountered was the extremely small time increment necessary due to the applied magnetic intensity having a period of 1/60 second. This in turn required a small increment in the space variable. Even then stability of the solution was not gained. An effort was made to normalize the time variable; however, the exact nature of the normalization needed was never clear.

Since it appeared that the time variable needed to be continuous, a study was made of the feasibility of solving the equation using an analogue computer. This method holds great promise, however the existing equipment available did not allow adequate representation of the non-linearity involved. It is of interest to note that there have been analogue computers* designed specificaly to solve this type problem.

*Dystac Analog Computer, Computer Systems, Inc.

IX. BIBLIOGRAPHY

Literature Cited

1. Brailsford, F., "Investigation of the Eddy-Current Anomaly in Electrical Sheet Steels", Journal I.E.E., 1948, Vol. 95, p. 38.
2. Newmann, E. A., "Magnetisch Hysteresis bei Wechselstrommagnetisierung", Zeitschrift fur Physik, 1933, Vol. 83, p. 619.
3. Churcher, B. G., "Testing Magnetic Sheet Steel", World Power, 1928, Vol. 9, p. 15.
4. Mac Lean, W., "Theory of Strong Electromagnetic Waves in Massive Iron", Journal of Applied Physics, 1954, Vol. 25, p. 1267.
5. Rosenberg, E., "Eddy-Currents in Solid Iron", Elektrotechnik und Machinenbau, 1923, Vol. 41, p. 317.
6. Habarland, G., Habarland, H., "Alternating Fields in Saturated Solid Iron", Archiv fur Elektrotechnik, 1930, Vol. 19, p. 126.
7. McConnell, H. H., "Eddy-Current Phenomena in Ferromagnetic Materials", AIEE Transactions, 1954, Vol. 73, p. 226.
8. Agarwal, P. D., "Eddy-Current Losses in Solid and Laminated Iron", AIEE Transactions, 1959, Vol. 78, p. 169.
9. Ramo, S., Whinnery, J. R., Fields and Waves in Modern Radio, John Wiley & Sons, Inc., New York, 1953, p. 241.

10. Dreyfus, L., "Flux distribution and Eddy-Current Losses in Armatures of Electric Machines", Archiv fur Electrotechnik, 1915, Vol. 4, p. 99.

11. Aspen, H., "Eddy-Currents in Solid Cylindrical Cores having Non-Uniform Permeability", Journal of Applied Physics, 1952, Vol. 23, p. 523.

12. Kescvamurthy, N., Rajagapalan, P. K., "Eddy-Currents in Solid Iron Due to Alternating Magnetic Flux", Procedings I.E.E., 1959, Monograph 339u, p. 207.

13. Pohl, R., "Electromagnetic and Mechanical Effects in Solid Iron Due to an Alternating or Rotating Magnetic Field", Procedings I.E.E., 1944, Vol. 91, p. 239.

14. Milne, W. E., Numerical Solution of Differential Equations, John Wiley & Sons, Inc., New York, 1953, p. 119.

Literature Examined

Agarwal, P. D., "Eddy-Current Losses in Solid and Laminated Iron", AIEE Transactions, 1959, Vol. 78, p. 169.

Aspen, H., "Eddy-Currents in Solid Cylindrical Cores haing Non-Uniform Permeability", Journal of Applied Physics, 1952, Vol. 23, p. 523.

Blake, L. R., "The Eddy-Current Anomaly in Ferromagnetic Laminae at High Rates of Change of Flux", Procedings I.E.E., Part II, Nov. 1949, Vol. 96, pp. 705-18.

Bozorth, R. M., Ferromagnetism, D. Van Nostrand Co., Inc., New York, N. Y., 1951.

Brailsford, F., "Investigation of the Eddy-Current Anomaly in Electrical Sheet Steels", Journal I.E.E., 1948, Vol. 95, p. 38.

Churcher, B. G., "Testing Magnetic Short Steel", World Power, 1928, Vol. 9, p. 15.

Concordia, C., "Synchronous Machine with Solid Cylindrical Rotor", AIEE Transactions, Part II, Vol. 78, pp. 1650-57.

Concordia, C., Poritsky, H., "Synchronous Machine with Solid Cylindrical Rotor", AIEE Transactions, Jan. 1937, Vol. 56, pp. 49-58.

Dreyfus, L., "Flux Distribution and Eddy-Current Losses in Armatures of Electric Machines", Archiv fur Eliktrotechnik, 1915, Vol. 4, p. 99.

Forsythe & Wasow, Finite Difference Methods for Partial Differential Equations, John Wiley & Sons, Inc., New York, 1960.

Habarland, G., Habarland, H., "Alternating Fields in Saturated Solid Iron", Archiv fur Elektrotechnik, 1930, Vol. 19, p. 126.

Hale, J. W., Richardson, F. R., "Mathematical Description of Core Losses", AIEE Transactions, Part I, Sept. 1953, Vol. 72, pp. 495-501.

Hammond, P., "Calculation of the Magnetic Field of Rotating Machines", Procedings I.E.E., May 1959, Monograph 333, pp. 158-64.

Kesevamurthy, N., Rajagapalan, P. K., "Eddy-Currents in Solid Iron Due to Alternating Magnetic Flux", Procedings I.E.E., 1959, Monograph 339u, p. 207.

Lee, E. W., "Eddy Current Effects in Rectangular Ferromagnetic Rods", Procedings I.E.E., Sept. 1960, Vol. 107c, pp. 257-64.

Mac Lean, W., "Theory of Strong Electromagnetic Waves in Massive Iron", Journal of Applied Physics, 1954, Vol. 25, p. 1267.

McConnell, H. M., "Eddy-Current Phenomena in Ferromagnetic Materials", AIEE Transactions, 1954, Vol. 73, p. 226.

McLachlan, N. W., Bessel Functions for Engineers, Oxford University Press, London, England, 1934.

Milne, W. E., Numerical Solution of Differential Equations, John Wiley & Sons, Inc., New York, 1953, p. 119.

Newmann, E. A., "Magnetisch Hysteresis bei Wechselstrommagnetisierung", Zeitschrift fur Physik, 1933, Vol. 83, p. 619.

Pohl, R., "Electromagnetic and Mechanical Effects in Solid Iron Due to an Alternating or Rotating Magnetic Field", Procedings I.E.E., 1944, Vol. 91, p. 239.

Ramo, S., Whinnery, J. R., Fields and Waves in Modern Radio, John Wiley & Sons, Inc., New York, 1953, p. 241.

Robertson, D. S., Elliott, D., "Magnetic Losses in Cores of Various Shapes", Nuclear Instrumentation and Methods, Sept. 1959, Vol. 5, No. 3, pp. 133-41.

Rosenberg, E., "Eddy-Currents in Solid Iron", Elektrotechnik und Machinenbau, 1923, Vol. 41, p. 317.

Schindler, M. J., "The Effect of Flux Distribution on Iron Losses", AIEE Transactions, Vol. 78, pp. 1069-74.

Wood, A. J., "Analysis of Solid Rotor Machines, Operational Impedances and Equivalent Circuit", AIEE Transactions, Part III, Vol. 78, pp. 1657-65.

X. ACKNOWLEDGEMENTS

The author wishes to express his appreciation to Dr. Richard T. Smith and Professor John P. Gordon, his thesis advisors, for the help and cooperation they gave him.

In addition, the author would like to express his gratitude to his wife, Faye, who typed and edited this manuscript.

XI. VITA

Earl Napoleon Fray was born on January 2, 1934 in Kennett, Missouri. He attended public schools in Kennett, Missouri and Memphis, Tennessee.

In February, 1951 he enlisted for two years in the United States Air Force. After his discharge in 1953 he was employed by the Memphis Furniture Manufacturing Company as Assistant Traffic Manager for two and one half years. In the Fall of 1955 he enrolled at Christian Brothers College in Memphis, Tennessee where he earned the Bachelor of Science Degree in Electrical Engineering in 1959.

After graduation he accepted a teaching position at the Virginia Polytechnic Institute in the Department of Electrical Engineering.

In 1953 he married Miss Faye Alston of Memphis, Tennessee and they now live in Blacksburg, Virginia with their three sons.

Earl N. Fray

POWER LOSSES IN MASSIVE, SOLID, SATURABLE IRON

by

Earl Napoleon Fray

Virginia Polytechnic Institute

Department of Electrical Engineering

MASTER OF SCIENCE THESIS

June, 1962

ABSTRACT

The losses in iron are generally considered to consist of two components--hysteresis loss and the loss due to eddy-currents. The classical formulae used to compute these losses, assume they are independent, however it is a well known fact that the experimentally determined loss is invariably greater than the computed loss when the above assumption is employed.

Some of the more significant contributions toward the removal of this anomaly are considered. These methods, in general, fail to consider all the factors which are known to contribute to this anomaly.

An exact solution to the field equation which governs these losses is not possible due to the extreme non-linear relation between the flux density and the magnetic intensity. An approximate solution to this problem is proposed which takes into account the effect of hysteresis as well as harmonics.